

RESEARCH

Open Access



UPLC–ESI–QTOF–MS profiling, antioxidant, antidiabetic, antibacterial, anti-inflammatory, antiproliferative activities and in silico molecular docking analysis of *Barleria strigosa*

Ming Lei¹, Lei Wang¹, Oladipupo Odunayo Olatunde², Sudarshan Singh³, Chitchamai Ovatlarnporn^{4,5}, Abdul Basit^{4,5} and Opeyemi Joshua Olatunji^{6*}

Abstract

Background This study investigated the in vitro antidiabetic, antioxidant, antibacterial, anti-inflammatory and anti-proliferative effects of *B. strigosa* hydrophilic (BSTR) and lipophilic (LSB) leaves extracts. The phytochemical profile was also performed using UHPLC–ESI–QTOF–MS.

Results The results indicated that BSTR and LSB showed excellent antioxidant properties in the DPPH scavenging, ABTS scavenging, FRAP and MCA assays. The extracts also demonstrated α -glucosidase (81.56–157.56 $\mu\text{g}/\text{mL}$) and α -amylase (204.44 $\mu\text{g}/\text{mL}$) inhibitory activities. In addition, the extracts showed significant cytotoxic and anti-proliferative effects against oral squamous carcinoma (CLS-354/WT) cancer cells. Furthermore, the extracts showed excellent antibacterial activity against *Listeria monocytogenes*, *Vibrio parahaemolyticus*, *Escherichia coli*, *Pseudomonas aeruginosa* and *Staphylococcus aureus*. Both extracts exhibited a significant reduction in nitric oxide secretion against activated macrophage cells. The UHPLC–MS analysis revealed that *B. strigosa* is rich in terpenoids, iridoid glycosides, flavonoids, and phenolic compounds. The plethora of these compounds may be responsible for the observed activities. In addition, the bioactive compounds identified by UHPLC–ESI–QTOF–MS were analyzed using silico molecular docking studies to determine the binding affinity with α -amylase and α -glucosidase.

Conclusions These results suggest that *B. strigosa* is an excellent pharmacological active plant and it provides the basis for further studies on the exploration of its potentials in oxidative stress induced disorders.

Keywords *Barleria strigosa*, Antioxidant, Antidiabetic, Anticancer activity, Antimicrobial

*Correspondence:

Opeyemi Joshua Olatunji
Joshua.OLATUNJI@um6p.ma

Full list of author information is available at the end of the article



© The Author(s) 2023, corrected publication 2023. **Open Access** This article is licensed under a Creative Commons Attribution 4.0 International License, which permits use, sharing, adaptation, distribution and reproduction in any medium or format, as long as you give appropriate credit to the original author(s) and the source, provide a link to the Creative Commons licence, and indicate if changes were made. The images or other third party material in this article are included in the article's Creative Commons licence, unless indicated otherwise in a credit line to the material. If material is not included in the article's Creative Commons licence and your intended use is not permitted by statutory regulation or exceeds the permitted use, you will need to obtain permission directly from the copyright holder. To view a copy of this licence, visit <http://creativecommons.org/licenses/by/4.0/>. The Creative Commons Public Domain Dedication waiver (<http://creativecommons.org/publicdomain/zero/1.0/>) applies to the data made available in this article, unless otherwise stated in a credit line to the data.

Graphical Abstract



Barleria strigosa extract

In vitro antioxidant studies

In vitro antidiabetic activity

Phytochemical analysis

In vitro anticancer activity

Antimicrobial activity

Introduction

From time immemorial, both traditional medicinal plants and natural products have played pivotal roles in primary healthcare. The use of natural products, especially medicinal plants in drug discovery has gained prominence in several developing countries, where accessibility to medicines and healthcare facilities is inadequate [1–3]. Medicinal plant extracts have been employed in several traditional medicine systems for thousands of years. The cocktail of bioactive compounds present in these extracts, including polyphenols, alkaloids, terpenes, steroids, and carotenoids, forms the basis of the synergistic and multiple mechanisms of therapeutic action displayed by these medicinal plant extracts. Furthermore, several biologically active compounds isolated from medicinal plants have become building blocks for the development of new leads, some of which have been approved or are undergoing various clinical trials [4, 5]. In addition, the excellent pharmacological properties including antioxidant, anti-inflammatory, anticancer, antidiabetic, antibacterial, and cytotoxic activities displayed by medicinal plants make them notable choices for pharmacological exploration [4–6]. In particular, antioxidant compounds/medicinal plants have shown promising effects against several chronic diseases, due to their ability to mitigate ROS and oxidative stress-induced disorders. As such, the discovery of new natural antioxidant agents will be of significant value in human health [7].

Barleria strigosa (family Acanthaceae) is a relatively unexplored medicinal plant found in tropical Asia [8]. Traditionally, *B. strigosa* is used for treating fever, flu,

nose bleeding and as an antidote for detoxification of poisons [8, 9]. Studies on the pharmacological and phytochemical profiles of *B. strigosa* are very limited, but it has been reported to exhibit antibacterial properties against *Bacillus subtilis*, *Staphylococcus aureus*, and *Micrococcus luteus* [10]. Regarding the phytochemical study on *B. strigosa*, only two reports are available on the bioactive compounds from the plant including phenylethanoid glycoside, iridoid glycoside, phenolic acid and flavonoids [8, 11, 12]. Due to the scanty information on the phytochemical and pharmacological activity of *B. strigosa*, proper phytochemical profiling may afford a better understanding of the therapeutic potentials of the plant to facilitate more effective usage. Therefore, this study investigated the UPLC–ESI–QTOF–MS profiling, antioxidant, antidiabetic, antibacterial, anti-inflammatory, and anti-cancer properties of extracts from *B. strigosa*.

Materials and methods

Chemicals and reagents

3-(4,5-Dimethylthiazol-2-yl)-2,5-diphenyltetrazolium bromide (MTT), gelatin, dimethyl sulfoxide, α -amylase enzyme, α -glucosidase enzyme, ethylenediaminetetraacetic acid (EDTA), 2,2-diphenyl-1-picrylhydrazyl (DPPH), 2,2-azino-bis-(3-ethylbenzothiazoline-6-sulfonic acid) diammonium salt (ABTS), ferric chloride, ferrous sulfate, Trolox and potassium persulfate were purchased from Sigma-Aldrich St. Louis, MO, USA. Fetal bovine serum (FBS), RPMI-1640, DMEM, N-(1-Nappthyl) ethylenediamine, 1% sulfanilamide, phosphoric acid, phosphate buffer saline, and penicillin/streptomycin (U/ml) were obtained

from Biochrom GmbH Berlin, Germany and PAA Laboratories GmbH, Pasching, Austria. L-glutamine, trypsin–EDTA, 2',7'-dichlorodihydrofluorescein diacetate were products of Gibco Life Technologies, Carlsbad, CA, USA. 4',6-Diamidino-2-phenylindole (DAPI) was purchased from Invitrogen, Eugene, USA. Oral squamous carcinoma cell line (CLS-354/WT) and macrophage cells (RAW 264.7) were obtained from the Department of Pharmaceutical Sciences, Faculty of Pharmacy, Chiang Mai University, Thailand. All other chemicals used were of analytical grade.

Plant material preparation and extraction

Freshly harvested leaves of *B. strigosa* were collected from Yala Province, Thailand in July 2020 and the botanical authentication of the plant was performed at the Faculty of Thai Traditional Medicine, Prince of Songkla University. The leaves of the plant were washed thoroughly under running tap water, oven-dried at 60 °C, and powdered. The powdered leaves (100 g) were macerated with 80% ethanol (1 L) for 24 h on a shaker (400 rpm) at room temperature. The extract was filtered, while the residue was re-macerated as stated above. Subsequently, the combined ethanolic extract was evaporated under reduced pressure to about 30% of its initial volume and the concentrate was left to stand at 4 °C overnight. Thereafter, the clear hydrophilic upper layer was decanted, centrifuged at 6000 rpm for 30 min, and lyophilized. The lyophilized hydrophilic sample was named “BSTR” and refrigerated until further use. The congealed lipophilic precipitate at the bottom of the container was also collected and lyophilized to obtain the lipophilic fraction and named “LSB”. The LSB extract was also refrigerated until further use [13–15].

Total phenolic content (TPC)

The TPC was performed using the Folin–Ciocalteu colorimetric assay according to a previous description [16, 17]. Briefly, 100 µL of the ethanolic extract solution of BSTR and LSB were mixed with 10% Folin–Ciocalteu reagent, vortexed and allowed to stand for 5 min. Afterwards, 750 µL of Na₂CO₃ solution was added, the mixture was vortexed and incubated in a dark environment for 2 h at room temperature. The absorbance of the solution was read at 765 nm. The standard curve was prepared from the absorbance readings of gallic acid (0–0.1 mg/mL). The

TPC was expressed as mg gallic acid equivalent (GE)/g dry extract.

Total flavonoid content (TFC)

The TFC was determined spectrophotometrically using an aluminum assay [16]. Briefly, 200 µL of BSTR and LSB ethanolic extract solution and 800 µL of distilled water were properly mixed in a 5 mL Eppendorf tube, followed by the addition of 60 µL of 5% NaNO₂ solution and 60 µL of 10% AlCl₃ solution. The resulting solution was allowed to stand for 5 min. Thereafter, 400 µL of 1 M NaOH solution and 2 mL of distilled water was added. The solution was vortexed, and the absorbance was read at 510 nm. The TFC was calculated and presented as milligram catechin equivalent per gram of extract (mg CE/g).

Antioxidant assays

The antioxidant activities of BSTR and LSB including DPPH (2,2-diphenyl-1-picrylhydrazyl) radical scavenging activity, ferric reducing antioxidant power (FRAP), ABTS radical scavenging activity (ABTS) and metal chelating activity (MCA) were determined using a previously described protocol [16]. DPPH, FRAP and ABTS activities were expressed as µmol Trolox equivalent (TE) g/ dry extract, while MCA was expressed as µmol EDTA equivalent (EE) g/ dry extract.

Alpha-glucosidase inhibitory activity

The inhibitory effect of the extracts on α-glucosidase enzyme was evaluated using the method of Kumar et al. [18], with some slight modifications. The extracts were solubilized in ethanol and diluted with 20 nM of phosphate buffer to concentrations ranging from 0.5 to 4000 µg/mL. The solubilized extracts were mixed with 0.57 U/mL of α-glucosidase enzyme solution (dissolved in 50 mM of phosphate buffer, pH 6.9) and the mixture was incubated at 37 °C for 15 min. After the incubation period, 50 µL of p-nitrophenyl-α-D-glucopyranoside was added and the solution was further incubated for 20 min. Thereafter, the reaction was quenched by adding 50 µL of 1 M Na₂CO₃ solution and the absorbance of the solution was measured at 405 nm. Acarbose was used as the standard drug, while phosphate buffer was used instead of the extract as negative control and the blank (without the α-glucosidase). The inhibitory effect of the extracts on α-glucosidase enzyme was expressed as IC₅₀ value and calculated using the following equation:

$$\% \text{ inhibition} = \left[\frac{A_{\text{control}} - (A_{\text{sample}} - A_{\text{blank}})}{A_{\text{control}}} \right] \times 100$$

A_{control} = absorbance of negative control.
 A_{sample} = absorbance of the sample.
 A_{blank} = absorbance of blank (without the enzyme).

Alpha-amylase inhibitory activity

The inhibitory effect of the extracts on α -amylase enzyme was evaluated using the method of Makinde et al. [19]. The reaction solution consisted of 50 μL of the extracts mixed with 20 μL of 1% starch solution and 20 μL of 20 mM phosphate buffer (pH 6.9). The solution was incubated at 37 °C for 3 min on a shaker. Thereafter, 20 μL of 12.8 U/mL of porcine pancreatic α -amylase solution was added and the mixture was further incubated at 37 °C for an additional 15 min. The reaction was terminated by adding 20 μL of 1 M HCl and 100 μL of iodine test solution (2.5 mM) was added. The absorbance of the solution was determined at 630 nm using a microplate reader. Acarbose was used as the positive standard. The inhibitory effect of the extracts on α -amylase enzyme was expressed as IC_{50} value and calculated using the following equation:

$$\% \text{ inhibition} = [A_{\text{control}} - (A_{\text{sample}} - A_{\text{blank}})/A_{\text{control}}] \times 100$$

A_{control} = absorbance of negative control.
 A_{sample} = absorbance of the sample.
 A_{blank} = absorbance of blank (without the enzyme).

Antibacterial activity

The minimum inhibitory concentration (MIC) and minimum bactericidal concentration (MBC) of the extracts were determined against five bacterial strains including *Listeria monocytogenes* F2365, *Vibrio parahaemolyticus* PSU.SCB.16S.14, *Escherichia coli* DMST 4212, *Pseudomonas aeruginosa* PSU.SCB.16S.11 and *Staphylococcus aureus* DMST 4745 according to the protocol reported by Odedina et al. [20]. Briefly, each bacterial culture prepared in tryptic soy broth was serially diluted to the final concentration of 10^6 CFU/ml. Thereafter, 100 μL of the extracts at different concentrations (0.13–8 mg/mL) were placed in a sterile 96-well flat bottom micro titre plate. Subsequently, 100 μL of the bacterial cells were inoculated in triplicates and incubated for 24 h at 37 °C. A sterile 0.85% normal saline solution (NSS) and Penicillin G were used instead of the extract as a negative and positive control, respectively. The MIC was defined as the least concentration that resulted in complete inhibition of noticeable growth in the micro titre plate. An aliquots of 10 μL from the wells displaying no visible growth were spotted on tryptic soy agar and the plates were incubated at 37 °C. for 24 h. The lowest concentration of the extracts inhibiting bacterial growth on the tryptic soy agar plates after incubation was adjudged as MBC.

Cell culture and viability assay

Macrophage cell viability was tested against BSTR and LSB using mitochondrial MTT assay [5]. Briefly, RAW 264.7 cells were cultured in high glucose DMEM supplemented with FBS (10%) and 100 $\mu\text{g}/\text{mL}$ streptomycin and 100 $\mu\text{g}/\text{mL}$ penicillin solution. Approximately 1×10^4 cells/mL were seeded in 96-well plate and incubated at 37 °C in an incubator humidified with 5% CO_2 at 37 °C. After 24 h of incubation, the culture medium was replaced with a fresh DMEM medium. BSTR and LSB were diluted in the well containing DMEM to yield final concentrations of 7.8–1000 $\mu\text{g}/\text{mL}$. RAW 264.7 cells without the extract were used as a negative control. After 24 h incubation, cells were evaluated for their viability by MTT assay at a wavelength of 560 nm using a multimode plate reader (BioTek, Vermont, USA). Furthermore, epithelium such as phenotype oral squamous carcinoma cell line (CLS-354/WT) was cultured in RPMI-1640 supplemented with 10% FBS, 1% penicillin–streptomycin and 2 mM L-glutamine, and incubated in a humidified incubator with 5% CO_2 and 37 °C. CLS-354/WT at

1×10^4 cells/mL were seeded in 96-well plates and incubated for 24 h. The cells were then treated with BSTR and LSB (12.5–1600 $\mu\text{g}/\text{mL}$) for 24 h. After the treatment, cell viability was measured using MTT assay, and the absorbance was read at 560 nm using a multimode plate reader (BioTek, Vermont, USA).

Anti-proliferative assay

The anti-migration effects of the cells treated with BSTR and LSB were evaluated using the in vitro scratch assay [5]. The cells were seeded at 3×10^4 cells/well in a 6-well plate for 24. Thereafter, a sterile pipette tip was used to scratch the surface of the cells to create a 1 mm width wound. The cells were washed with PBS, and replaced with a fresh medium of extracts or RPMI-1640 medium as negative control. Cell migration images were taken at two timepoints (0 and 24 h) under a microscope and the residual gap between migrating cells was quantified using Image J software.

Nitrite production measurement

The method of Singh et al. [21] was used for the determination of nitrite production. Briefly, RAW 264.7 cells were cultured in DMEM medium supplemented with FBS (10%) and 1% penicillin/streptomycin. The cells were maintained at 37 °C in 95% humidity with 5% CO_2 . The cells (1×10^4 cells/mL) were seeded in a 96-well plate and

Table 1 Chemical profile of bioactive compounds present in *B. strigosa* extract using UPLC–ESI–QTOF–MS analysis

No	RT (min)	Mass (m/z)	Molecular formular	DB Diff (ppm)	Tentative compound identity
1	1.759	126.0315	C ₆ H ₆ O ₃	1.89	Larixinic acid
2	1.763	366.0745	C ₂₀ H ₁₄ O ₇	-1.51	Daphnoretin methyl ether
3	1.923	295.1066	C ₁₄ H ₁₇ NO ₆	-3.46	Sambunigrin
4	1.930	143.0951	C ₇ H ₁₃ NO ₂	-3.16	3β,6β-Dihydroxynortropane
5	5.407	364.1369	C ₁₅ H ₂₄ O ₁₀	0.13	Dihydrocatalpol
6	11.339	338.1003	C ₁₆ H ₁₈ O ₈	0.30	Hydrojuglone glucoside
7	12.155	224.0683	C ₁₁ H ₁₂ O ₅	0.64	5-(3',4',5'-Trihydroxyphenyl)-gammavalerolactone
8	12.349	314.1001	C ₁₄ H ₁₈ O ₈	0.20	Alopecuquinone
9	12.714	484.3035	C ₂₆ H ₄₄ O ₈	0.23	Goshonoside F2
10	13.147	644.3401	C ₃₂ H ₅₂ O ₁₃	1.01	Goshonoside F3
11	13.239	284.1258	C ₁₄ H ₂₀ O ₆	0.59	2-Phenylethyl beta-D-glucopyranoside
12	14.273	336.23	C ₂₀ H ₃₂ O ₄	0.31	16,17-Dihydroxy-16beta-(L)-kauran-19-oic acid
13	16.12	595.1661	C ₂₇ H ₃₁ O ₁₅	0.31	Pelargonidin 3,7-di-glucoside
14	16.141	608.1379	C ₂₇ H ₂₈ O ₁₆	-0.32	6''-(4-Carboxy-3-hydroxy-3-methylbutanoyl)hyperin
15	16.142	462.0795	C ₂₁ H ₁₈ O ₁₂	0.70	3-Methylellagic acid 8-rhamnoside
16	16.151	510.1734	C ₂₄ H ₃₀ O ₁₂	0.56	Plumerubroside
17	16.295	194.0578	C ₁₀ H ₁₀ O ₄	0.49	Isoferulic acid
18	16.569	370.1993	C ₁₉ H ₃₀ O ₇	-0.29	(3S,7E,9S)-9-Hydroxy-4,7-megastigmadien-3-one 9-glucoside
19	16.57	208.1462	C ₁₃ H ₂₀ O ₂	0.69	(5α,8β,9β)-5,9-Epoxy-3,6-megastigmadien-8-ol
20	16.726	504.27	C ₂₈ H ₄₀ O ₈	4.59	Ixocarpalactone A
21	16.733	499.3142	C ₂₆ H ₄₅ NO ₈	0.54	18-O-Methyldeleterine
22	16.780	372.215	C ₁₉ H ₃₂ O ₇	-0.54	Icariside B9
23	16.789	192.1512	C ₁₃ H ₂₀ O	1.33	2,4-Diisopropyl-3-methylphenol
24	16.811	512.2626	C ₂₆ H ₄₀ O ₁₀	-0.97	Andrographoside
25	16.848	468.1634	C ₂₂ H ₂₈ O ₁₁	-0.44	Prim-O-glucosylcimifugin
26	16.892	530.2725	C ₂₆ H ₄₂ O ₁₁	0.34	Cinnassiol D2 glucoside
27	16.975	386.1938	C ₁₉ H ₃₀ O ₈	0.79	Roseoside
28	17.008	328.1154	C ₁₅ H ₂₀ O ₈	1.30	Androsin
29	17.008	490.1451	C ₂₄ H ₂₆ O ₁₁	4.97	Andrographidine E
30	17.009	936.3257	C ₄₄ H ₅₆ O ₂₂	0.63	Epimedokoreanoside I
31	17.010	468.1629	C ₂₂ H ₂₈ O ₁₁	0.65	6-O-p-Hydroxybenzoyl ajugol
32	17.046	402.1887	C ₁₉ H ₃₀ O ₉	0.60	Spionoside B
33	17.055	358.090	C ₁₅ H ₁₈ O ₁₀	-0.05	Dihydrocaffeic acid 3-O-glucuronide
34	17.063	524.2259	C ₂₆ H ₃₆ O ₁₁	-0.35	(8R,8'R)-Secoisolariciresinol 9-glucoside
35	17.121	286.2297	C ₂₀ H ₃₀ O	-0.19	(+)-Totarol
36	17.122	650.3277	C ₃₄ H ₅₀ O ₁₂	3.91	Thapsigargin
37	17.122	666.2938	C ₃₉ H ₄₂ N ₂ O ₈	0.48	Thalpinine
38	17.123	628.3457	C ₃₂ H ₅₂ O ₁₂	0.35	Ecdysterone-3-O-beta-D-glucopyranoside
39	17.187	498.1373	C ₂₂ H ₂₆ O ₁₃	0.02	Verproside
40	17.196	422.2154	C ₁₉ H ₃₄ O ₁₀	-0.58	1-Octen-3-ol-3-o-beta-D-xylopyranosyl(1->6)-beta-D-glucopyranoside
41	17.272	642.3247	C ₃₂ H ₅₀ O ₁₃	0.64	Steviobioside
42	17.287	494.1788	C ₂₄ H ₃₀ O ₁₁	0.11	Harpagoside
43	17.329	498.283	C ₂₆ H ₄₂ O ₉	-0.20	Isodopharicin F
44	17.340	482.1424	C ₂₂ H ₂₆ O ₁₂	-0.01	Catalposide
45	17.342	368.1473	C ₁₈ H ₂₄ O ₈	-0.60	Methyl (R)-9-hydroxy-10-undecene-5,7-dienoate glucoside
46	17.343	342.095	C ₁₅ H ₁₈ O ₉	0.30	Glucocaffeic acid
47	17.343	148.0526	C ₉ H ₈ O ₂	-0.97	E-Cinnamic acid
48	17.367	634.3327	C ₃₄ H ₅₀ O ₁₁	4.09	(3b,20R,22R)-3,20,27-Trihydroxy-1-oxowitha-5,24-dienolide 3-glucoside
49	17.438	536.2596	C ₂₈ H ₄₀ O ₁₀	4.79	7β-Hydroxy-7-desacetoxykhivorinic acid, methyl ester

Table 1 (continued)

No	RT (min)	Mass (m/z)	Molecular formular	DB Diff (ppm)	Tentative compound identity
50	17.439	514.2779	C ₂₆ H ₄₂ O ₁₀	-0.17	Cofaryloside
51	17.548	348.1937	C ₂₀ H ₂₈ O ₅	-0.09	Longikaurin A
52	17.597	512.1531	C ₂₃ H ₂₈ O ₁₃	-0.12	3-(4-Hydroxy-3-methoxyphenyl)-1,2-propanediol 2-O-(galloyl-glucoside)
53	17.669	292.1164	C ₁₂ H ₂₀ O ₈	-1.84	Pantoyllactone glucoside
54	17.670	426.2408	C ₂₆ H ₃₄ O ₅	-0.30	Dihydro-7-desacetyldeoxygedunin
55	17.670	316.204	C ₂₀ H ₂₈ O ₃	-0.53	Lagaspholones A
56	17.671	462.2621	C ₂₆ H ₃₈ O ₇	-0.84	10-Desacetyltaxuyunnanin C
57	17.743	630.3607	C ₃₂ H ₅₄ O ₁₂	1.37	Lyciumoside I
58	17.764	458.247	C ₃₀ H ₃₄ O ₄	-2.79	Sophoranochromene
59	17.789	572.3095	C ₃₁ H ₄₄ N ₂ O ₈	0.43	Isodelectine
60	17.867	480.1631	C ₂₃ H ₂₈ O ₁₁	0.04	Albiflorin R1
61	17.904	332.1989	C ₂₀ H ₂₈ O ₄	-0.28	Hautriwaic acid
62	17.911	756.3551	C ₃₇ H ₅₆ O ₁₆	2.30	Rhodexin D
63	17.935	348.1934	C ₂₀ H ₂₈ O ₅	0.65	Novaxenicins A
64	18.011	660.2757	C ₃₄ H ₄₄ O ₁₃	3.80	Taccalonolide J
65	18.114	316.2041	C ₂₀ H ₂₈ O ₃	-0.79	Lagaspholones A
66	18.123	1572.759	C ₇₆ H ₁₁₆ O ₃₄	-15.36	Protocrocin
67	18.124	282.1979	C ₂₀ H ₂₆ O	1.82	Juvocimene 1
68	18.128	492.2366	C ₂₆ H ₃₆ O ₉	-1.33	Caryoptin
69	18.160	560.3347	C ₃₂ H ₄₈ O ₈	0.39	Dihydroisocucurbitacin-beta-25-acetate
70	18.203	708.3326	C ₃₆ H ₅₂ O ₁₄	4.42	Scillipheosidin 3-[glucosyl-(1->2)-rhamnoside]
71	18.252	548.2626	C ₂₉ H ₄₀ O ₁₀	-0.82	Archangelolide
72	18.273	506.216	C ₂₆ H ₃₄ O ₁₀	-1.66	Massonanoside C
73	18.481	479.2877	C ₂₆ H ₄₁ NO ₇	1.31	Delbruline
74	18.445	564.291	C ₃₀ H ₄₄ O ₁₀	4.39	Strophanthidin-beta-D-digitaloside
75	18.446	346.1779	C ₂₀ H ₂₆ O ₅	0.34	Rabdoserrin A
76	18.642	478.2209	C ₂₅ H ₃₄ O ₉	-1.31	Simalikilactone D
77	18.751	552.185	C ₂₆ H ₃₂ O ₁₃	-1.26	Durantoside I
78	18.926	544.3399	C ₃₂ H ₄₈ O ₇	0.20	Hovenidulcigenin A
79	19.321	474.2255	C ₂₆ H ₃₄ O ₈	-0.35	Nigakilactone G
80	20.296	623.4035	C ₃₄ H ₅₇ NO ₉	-0.22	Pingbeidinoside
81	21.243	576.1262	C ₃₀ H ₂₄ O ₁₂	0.93	Epicatechin-(2beta->5,4beta->6)-entepicatechin
82	21.293	310.1571	C ₂₀ H ₂₂ O ₃	-0.53	2,3-Dehydrosalvipipone

incubated till the formation of a monolayer. After the formation of a confluent monolayer, the cells were at various concentrations (3.9–500 µg/ml) of BSTR and LSB in the presence and absence of 50 ng/mL lipopolysaccharide (LPS) for 18 h. The culture supernatant (75 µL) collected after treatment was mixed with equal volume (75 µL) of Griess reagent (1:1 ratio of 0.1% N-(1-Napthyl) ethylenediamine and 1% sulfanilamide in 5% phosphoric acid) and incubated at room temperature for 30 min. The optical density of the solution was measured at 540 nm using a microplate reader (BioTek, Vermont, USA) to estimate nitric oxide (NO) concentrations (%) in samples and standards. The nitrite level was quantified using nitrite standard curve ($Y=0.0115+0.0418x$; $r^2=0.9998$). The

data were expressed as a percentage (%) of nitrite levels secreted by treated cells relative to control (LPS-treated cells). After treatment with Griess reagent, cell viability was measured using MTT assay. Briefly, the spent media was replaced with an equal volume of serum-free DMEM containing MTT solution (0.5 mg/mL) and incubated for 3 h. The quantity of formazan was measured by recording the changes in the absorbance at 560 nm using a microplate reader (BioTek, Vermont, USA).

Analysis of cell death by nuclear staining

The nuclear morphology of the cells after exposure to BSTR and LSB was observed for cell apoptosis using a previously reported method [21]. Cells (1×10^4 cells/well)

Table 2 Antioxidant activity of *B. strigosa* extracts

Sample/assay	SBTR	LSB
DPPH ($\mu\text{mol TE/g}$ dry extract)	21.99 \pm 0.12 ^a	4.48 \pm 0.51 ^b
ABTS ($\mu\text{mol TE/g}$ dry extract)	244.90 \pm 5.39 ^a	235.98 \pm 10.72 ^b
FRAP ($\mu\text{mol TE/g}$ dry extract)	107.80 \pm 1.94 ^a	91.92 \pm 2.34 ^b
MCA ($\mu\text{mol EDTA/g}$ dry extract)	8.69 \pm 0.43 ^a	2.68 \pm 0.11 ^b
TPC (mg GAE/g dry extract)	50.26 \pm 3.07	41.83 \pm 16.96
TFC (mg CE/g dry extract)	14.76 \pm 0.46 ^a	7.08 \pm 0.46 ^b

Different lowercase superscripts within the same row indicate significant difference at $p < 0.05$

were plated on 0.1% v/v gelatin coated coverslip and subsequently treated with BSTR and LSB at IC₅₀ values (50% inhibition of CLS-354/WT growth) or with RPMI-1640 culture media as a negative control for 24 h. The cells were washed with PBS, fixed with pre-cooled ($-20\text{ }^{\circ}\text{C}$) acetone for 5 s followed by methanol for 10 s, and stained with DAPI for 15 min. The cells were examined under fluorescence Olympus-DP74 inverted microscope (Olympus Tokyo, Japan) with ultraviolet light excitation wavelength at 358 nm and emission wavelength at 461 nm.

UPLC–ESI–QTOF–MS analysis

BSTR was chosen for the UPLC–ESI–QTOF–MS analysis due to its superior biological effects in the assays conducted. 50 mg of BSTR powder was solubilized in 70% methanol and the resulting solution was vortexed and filtered using a 0.2 μm membrane syringe filter (Merck Millipore). The clear solution of BSTR was subjected to UPLC–ESI–QTOF–MS analysis following previously reported procedures and parameters [5].

Bioinformatics analysis

Molecular docking studies

In the molecular docking analysis, five predominant compounds from the UPLC–QTOF–ESI–MS profile were docked against α -glucosidase and α -amylase enzymes. The structures of α -amylase (PDB Id: 4GQR) and α -glucosidase (PDB Id: 5NN5) were downloaded from the protein database (<http://www.rcsb.org/pdb>) in PDB format. All the water molecules, existing ligands, and non-essential protein entities were removed. The Discovery Studio 2021 client software of the ligands, namely, acarbose (standard), (3S,7E,9S)-9-hydroxy-4,7-megastigmadien-3-one 9-glucoside, (5a,8b,9b)-5,9-epoxy-3,6-megastigmadien-8-ol, ixocarpalactone A, plumerubroside and isoferulic acid, was downloaded from the PubChem database bearing PubChem CIDs 11774, 131752058, 101415508, 327287, 44257126 and 736186, respectively. All the structures were prepared by

the addition of a polar “H” atom and energy minimization using Discovery Studio 2021 client software. The prepared receptors and ligands were then uploaded on Vina, which was embedded in PyRx. These structures were placed in the active pockets using AutoDock Vina. The interactions were evaluated using Discovery Studio Visualizer [22, 23].

Evaluation of ADMET profile

On 10th May 2023 SwissADME was accessed for the predictive estimation of the ADMET properties of the selected bioactive compounds [23]. Similarly, PROTOX-II was employed for the theoretical determination of the toxicity profile of the compounds [24].

Statistical analysis

The results were expressed as mean \pm SD and statistical analysis was performed using one-way ANOVA followed by Dunnett’s test on GraphPad Prism 8 (GraphPad Software Inc., CA, USA). Differences of $p < 0.05$ were considered statistically significant.

Results and discussion

Phytochemical profile

The species in the genus *Barleria* are well-known for their rich array of secondary metabolites, such as terpenoids, quinones, flavonoids, iridoids, and phenylethanoid glycosides, with notable biological activities including antimicrobial, anti-inflammatory, anticancer, antidiabetic, antiulcer, neuroprotective, hepatoprotective, analgesic, anti-arthritic and antihypertensive properties [12]. Thus, it is imperative to evaluate a detailed phytochemical profile of the leaves of *B. strigosa*. The LC–ESI–QTOF–MS analysis of BSTR exhibited a rich phytochemical composition from diverse phytochemical families. The tentatively characterized compounds along with their retention times, molecular formula, molecular ions, and assigned identities are presented in Table 1. A total of 82 compounds were detected in the BSTR extract. The individual compounds in the BSTR extract were tentatively identified using the QTOF–MS analysis (negative ionization mode) with an accuracy error less than 5 ppm

Table 3 In vitro antidiabetic activity of *B. strigosa* extracts

Sample/assay	SBTR	LSB	Acarbose
α -Glucosidase ($\mu\text{g/mL}$)	81.56 \pm 2.71 ^a	204.11 \pm 0.95 ^b	502.48 \pm 1.95 ^c
α -Amylase ($\mu\text{g/mL}$)	157.65 \pm 1.22 ^a	NA	17.28 \pm 0.05 ^b

Data are expressed as mean \pm SD ($n = 3$) and analyzed via one-way ANOVA with Dunnett’s test. Different lowercase superscripts within the same row indicate significant difference at $p < 0.05$. NA not active

(Table 1). Furthermore, the retention times, detected accurate mass, molecular formula and mass error of each of the tentatively identified compounds provided in Table 1 enhanced the characterization of the compounds [5, 6, 13]. Terpenoids including diterpenes, diterpene lactones, diterpene glycosides, iridoid glycosides were the prevailing class of compounds putatively identified in BSTR. Out of the 38 terpenoids detected in BSTR, 15 were diterpenes including (+)-totarol, isodopharicin F, longikaurin A, massonianoside C, caryoptin and hautriwaic acid. A number of diterpene lactones and diterpene glycosides including thapsigargin, archangelolide, nigakilactone G, goshonoside F2 and steviobioside were also identified in the extract. Three sesquiterpenes derivatives, namely, roseoside, thapsigargin, and archangelolide, were identified in BSTR.

In terms of flavonoids, the leaves of *Barleria* spp. are also known to be a reservoir of polyphenolic compounds, notably phenolics and flavonoids [11, 12]. In BSTR, four flavonoids were identified as 6''-(4-carboxy-3-hydroxy-3-methylbutanoyl)hyperin, plumerubroside, sophoranochromene and epicatechin-(2beta->5,4beta->6)-entepicatechin, while four phenolic glycoside, namely, hydrojuglone glucoside, dihydro-caffeic acid 3-O-glucuronide, glucocaffeic acid, and 3-(4-hydroxy-3-methoxyphenyl)-1,2-propanediol 2-O-(galloyl-glucoside), were detected. Six iridoid

glycosides; dihydrocatalpol, 6-O-p-hydroxybenzoyl aju-gol, verprosides, harpagoside, catalposide and durantoside I were also identified in the extract. Iridoid glycosides have previously been reported from the leaves of *Barleria* sp. [8, 12].

One tropane alkaloid (3β,6β-dihydroxynortropane), one anthocyanin glycoside (pelargonidin-3,7-di-glucoside), one naphthoquinone (2,3-dehydrosalvipisone), two norditerpenoid alkaloids (18-O-methyldebruline and debruline), one hydroxycinnamic acid (isoferulic acid), one phenylpropanoid (Icariside B9), one coumarin (daphnoretin methyl ether) were also putatively identified in BSTR (Table 1). Although our results on the phytochemical composition of *B. strigosa* is consistent with the class of compounds previously isolated from the plant, this study provides the first and extensive list of constituents from the leaves of the plant.

Antioxidant capacity

The total phenolic content (TPC) and total flavonoid content (TFC) of BSTR and LSB extracts are summarized in Table 2. BSTR and LBS showed relatively high TPC of 50.26 ± 3.07 and 41.83 ± 16.96 mg GAE/g, respectively, while the TFC were 14.76 ± 0.46 and

Table 4 Antimicrobial activity of *B. strigosa* extracts

Samples	MIC (mg/mL)					MBC (mg/mL)				
	LM	VP	PA	SA	EC	LM	VP	PA	SA	EC
BSTR	0.16 ^a	0.16 ^a	0.08 ^a	0.31	0.31 ^a	0.31 ^a	0.31 ^a	0.08 ^a	0.62 ^a	0.62 ^a
LSB	0.62 ^b	0.31 ^b	0.16 ^b	0.31	0.62 ^b	1.25 ^b	0.62 ^b	0.31 ^b	1.25 ^b	1.25 ^b

LM *Listeria monocytogenes* F2365, VP *Vibrio parahaemolyticus* PSU.SCB.165.14, PA *Pseudomonas aeruginosa* PSU.SCB.165.11, SA *Staphylococcus aureus* DMST 4745, *Escherichia coli* DMST 4212., MIC minimum inhibitory concentration, MBC minimum bactericidal concentration

Data are expressed as mean ± SD (n = 3) and analyzed via one-way ANOVA with Dunnett's test

Different lowercase superscripts within the same column indicate significant difference at p < 0.05

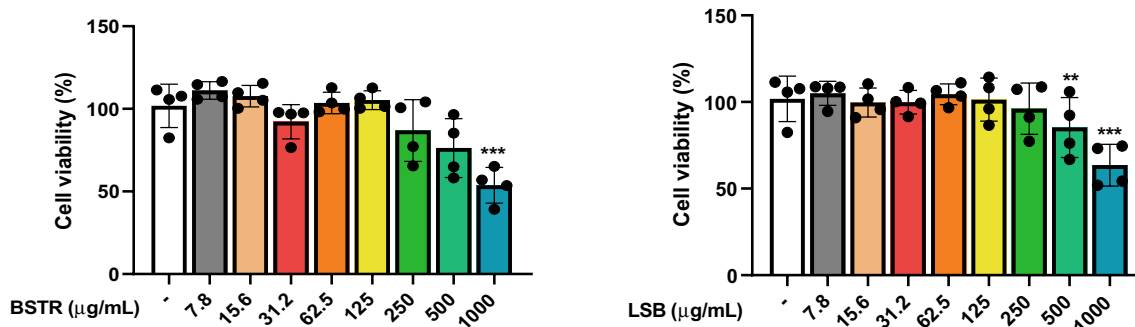


Fig. 1 Effect of BSTR and LSB on the macrophage cell viability. Data are expressed as mean ± SD from at least three independent experiments and analyzed via one-way ANOVA with Dunnett's test. **p < 0.01, ***p < 0.001 vs untreated control

7.08 ± 0.46 mg catechin/g, respectively. Furthermore, the in vitro antioxidant activities of BSTR and LSB were evaluated via radical scavenging, reducing power and metal chelating assays. The results showed that the DPPH and ABTS radical scavenging activities of BSTR were 21.99 ± 0.12 μmol TE/g and 244.90 ± 5.39 μmol TE/g, respectively, while that of LSB were 4.48 ± 0.51 and 235.98 ± 10.72, respectively (Table 2). Furthermore, the reducing power activity of BSTR and LSB in the FRAP assay were 107.80 ± 1.94 and 91.92 ± 2.34 μmol TE/g, respectively. While the metal chelating activity (MCA) of BSTR and LSB were 8.69 ± 0.43 and 2.68 ± 0.11 μmol EDTA-g, respectively (Table 2). Antioxidants play critical roles in the body’s defense against oxidative insults. Numerous studies have highlighted the role of oxidative stress in several diseases including diabetes, obesity, Alzheimer, cancer, and the impact of antioxidant plants, and compounds in the mitigation of these disorders [25, 26]. The ability of a sample to scavenge free radicals is extensively used in assessing the antioxidant capacity of natural products. Particularly, the DPPH and ABTS radical assays are based on the capability of the pharmacological agent to donate

hydrogen atoms/electrons to free radicals, thus stabilizing and halting the reactive chain [13, 15]. The MCA and FRAP antioxidant assay reflect the ability of the sample to reduce metal complex and it is associated with cellular antioxidant activity [16]. Therefore, the high antioxidant activities of SBTR and LSB extracts reflect the bioactive compounds identified in the extract via LC–MS, and since oxidative stress is a vital factor driving several chronic disorders. Hence, the antioxidant properties of the extract suggest its potential against oxidative damage.

In vitro antidiabetic activity

Diabetes is the most common metabolic disease, and it has emerged as a major public health concern owing to its prevalence and ensuing complications [27, 28]. In the last decade, there has been a 47% increase in the number of diabetic patients (366 million people in 2011 and 537 million people in 2021), and it is expected that there would be an additional 46% increase in the number of people living with diabetes by 2045 (783 million people). Diabetes is characterized by excessive blood glucose concentration due to insulin resistance and altered insulin

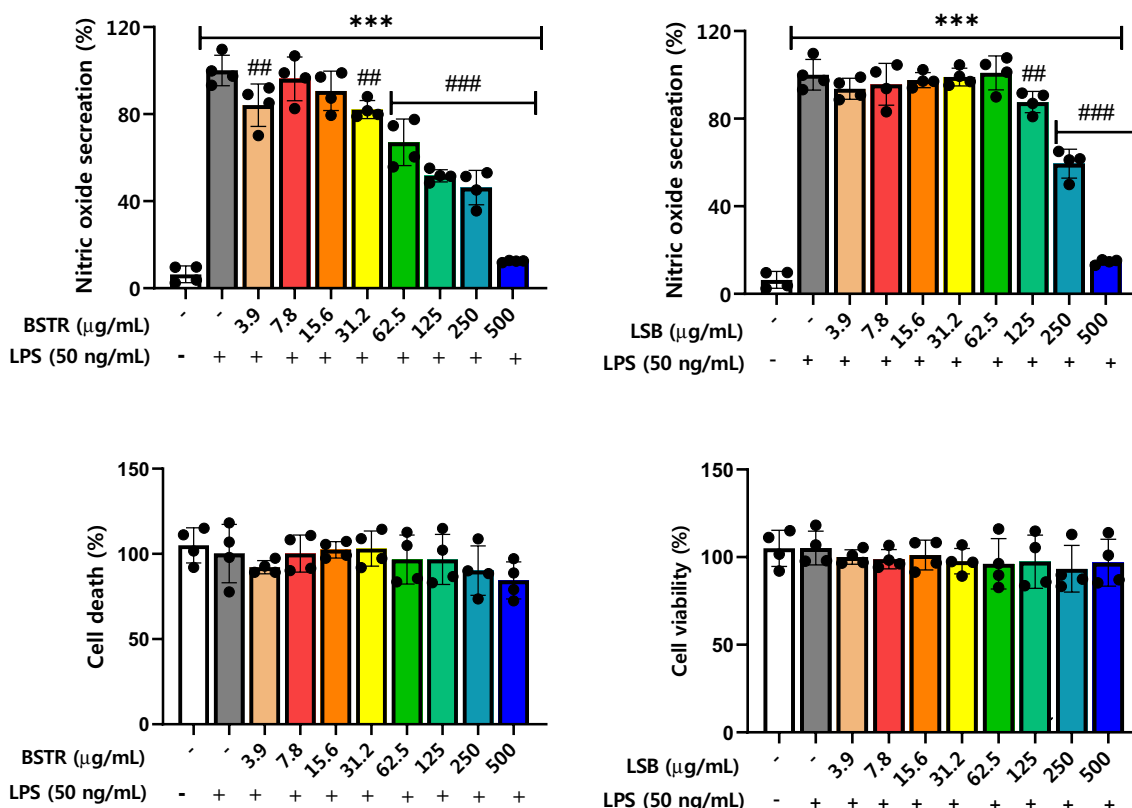


Fig. 2 Effect of BSTR and LSB on nitric oxide secretion and RAW 264.7 cells viability upon stimulation with lipopolysaccharides (50 ng/mL). Data are expressed as mean ± SD from at least three independent experiments and analyzed via one-way ANOVA with Dunnett’s test. ***p < 0.001 vs untreated control. ##p < 0.05, ###p < 0.001 vs lipopolysaccharides stimulated group

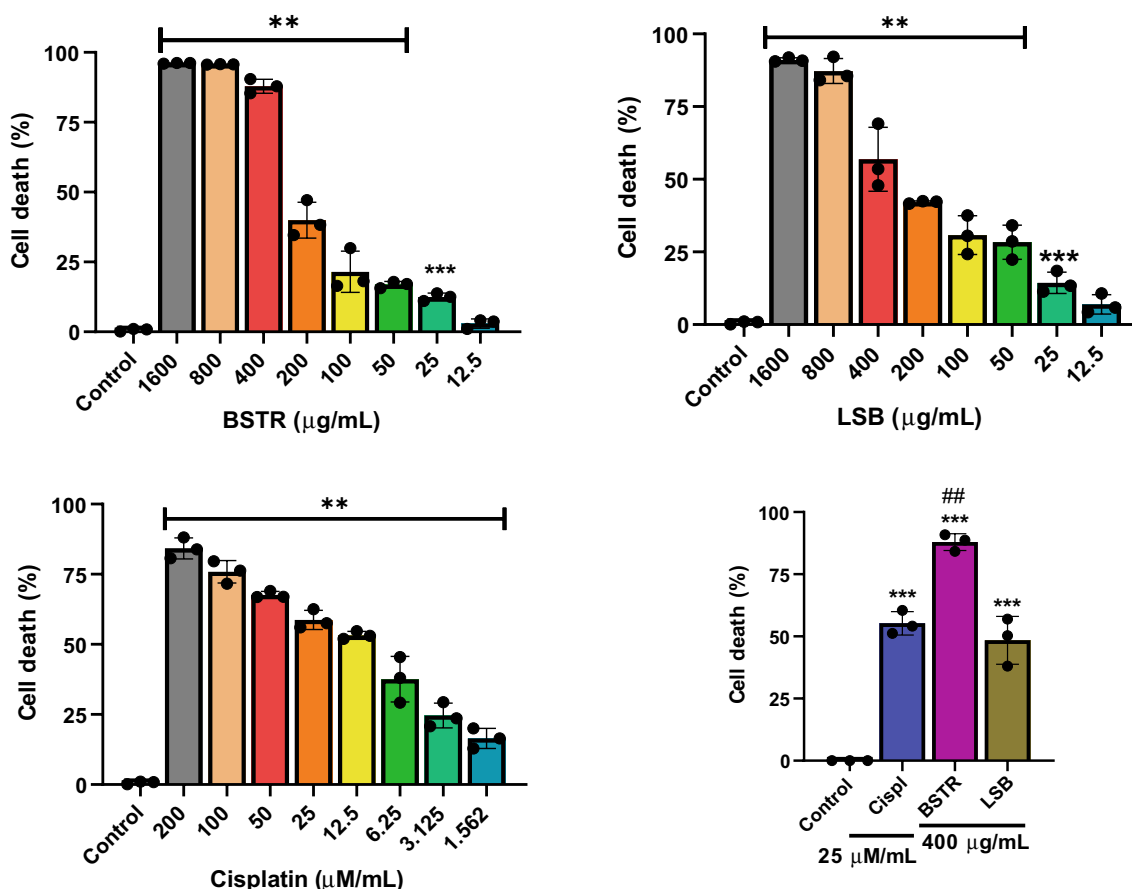


Fig. 3 Effect of *B. strigosa* extract and cisplatin on epithelium-like phenotype oral squamous carcinoma cell (CLS-354/WT) death. Data are expressed as mean ± SD from at least three independent experiments and analyzed via one-way ANOVA with Dunnett’s test. ****p* < 0.01, ***p* < 0.001 vs untreated control. ##*p* < 0.001 vs cisplatin

secretion from the pancreatic beta cells [27]. The absorption of glucose from the intestinal wall through the action of digestive enzymes (α -amylase and α -glucosidase) on carbohydrates results in hyperglycemia. Therefore, limiting the activities of these enzymes is an effective approach to relieve hyperglycemia [29–31]. On the other hand, oxidative stress has been extensively implicated in the pathogenesis of diabetes and several molecular mechanisms implicated in diabetic complication have been wholly or partly linked to increased reactive oxygen species, oxidative stress, and depleted antioxidant defense [13, 32]. As such, therapies that confer antioxidant, α -glucosidase, and α -amylase inhibitory properties may have a beneficial effect in the management of diabetes. As shown in Table 3, BSTR and LSB showed inhibitory effect against α -glucosidase enzyme at IC_{50} values of 81.56 and 204.11 μ g/mL, respectively, while the α -amylase inhibitory effect of BSTR was 157.65 μ g/mL. The extracts showed better efficacy than the standard drug acarbose.

Antimicrobial activity

Antimicrobial resistance has become a major public health concern due to the abuse of antibiotics and bacterial resistance, which has grossly increased the incidence of bacterial infectious illnesses and other opportunistic infections [32]. In view of this, phytochemicals have been extensively explored as potent antibacterial agents [19, 33]. The minimum inhibitory concentration (MIC) and minimum bactericidal concentration (MBC) of BSTR and LSB against gram-positive and gram-negative bacteria including *Listeria monocytogenes* F2365, *Vibrio parahaemolyticus* PSU.SCB.16S.14, *Escherichia coli* DMST 4212, *Pseudomonas aeruginosa* PSU.SCB.16S.11 and *Staphylococcus aureus* DMST 4745 are shown in Table 4. The MIC values of BSTR and LSB against *L. monocytogenes*, *V. parahaemolyticus*, *E. coli*, *P. aeruginosa*, and *S. aureus* were 0.16 and 0.62; 0.16 and 0.31; 0.31 and 0.62; 0.08 and 0.16; 0.31 and 0.31 mg/mL, respectively, while the MBC values for both extracts were 0.31 and

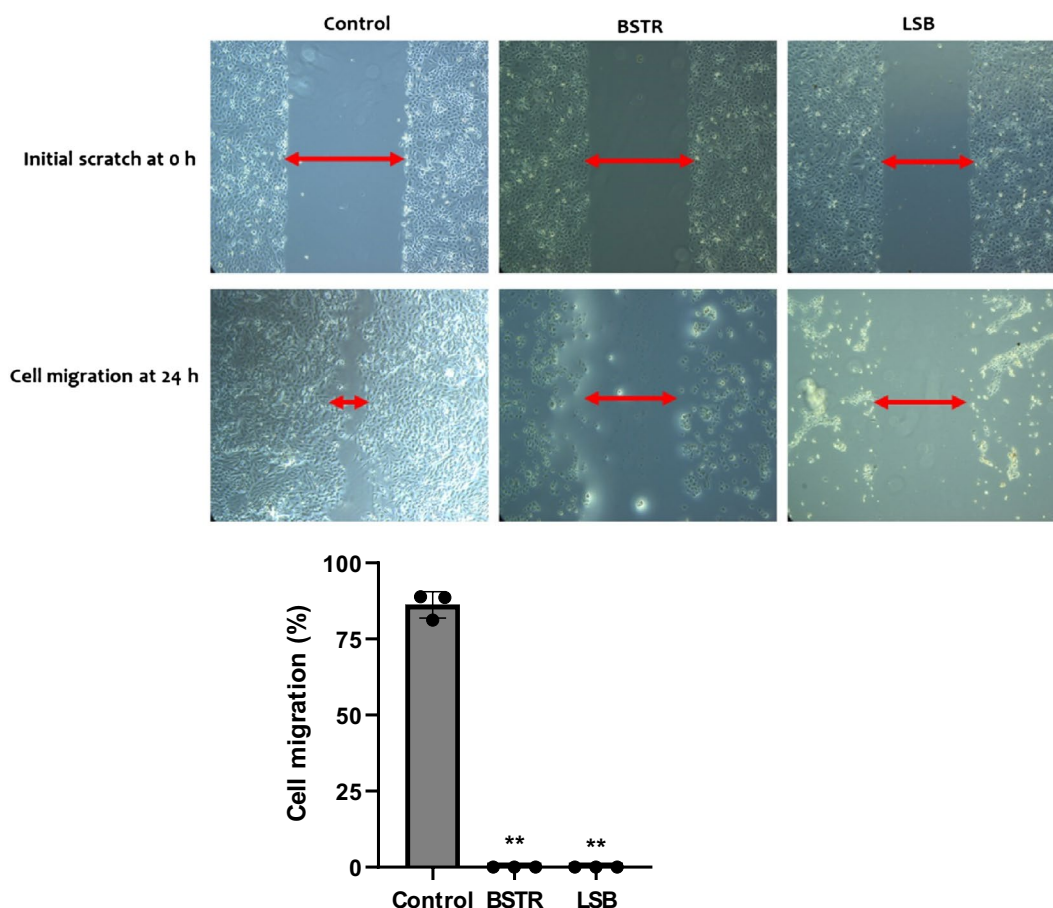


Fig. 4 Effect of *B. strigosa* on the percentage migration rate of epithelium-like phenotype oral squamous carcinoma cell (CLS-354/WT). Data are expressed as mean ± SD (n = 3) and analyzed using one-way ANOVA followed by Dunnett’s test. **p < 0.001 vs. untreated control

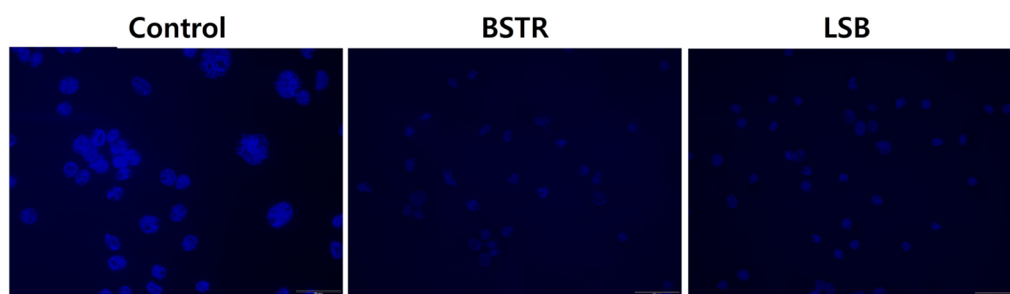


Fig. 5 Effect of *B. strigosa* on apoptosis by nuclear staining using DAPI nucleus staining

1.25; 0.31 and 0.62; 0.62 and 1.25; 0.08 and 0.16; 0.62 and 1.25 mg/mL, respectively (Table 4). In general, both BSTR and LSB showed promising antimicrobial activities towards the tested bacteria. This can be attributed to the richness of the diverse polyphenolic compounds in the extract. These compounds have been reported to render cell membranes permeable and/or disrupt the cell structure via the interaction with the cell membrane

(hydrophobic–hydrophobic activity interaction [34]. The excessive leakage of the critical ions and molecules from the cell via the interaction with the polyphenols leads to stress and ultimately cell death. Similar observations were reported when ethanolic extract of guava leaves and coconut husks were used to inhibit the proliferation of both gram-positive and gram-negative bacteria [15, 16]. It was also observed that BSTR showed higher

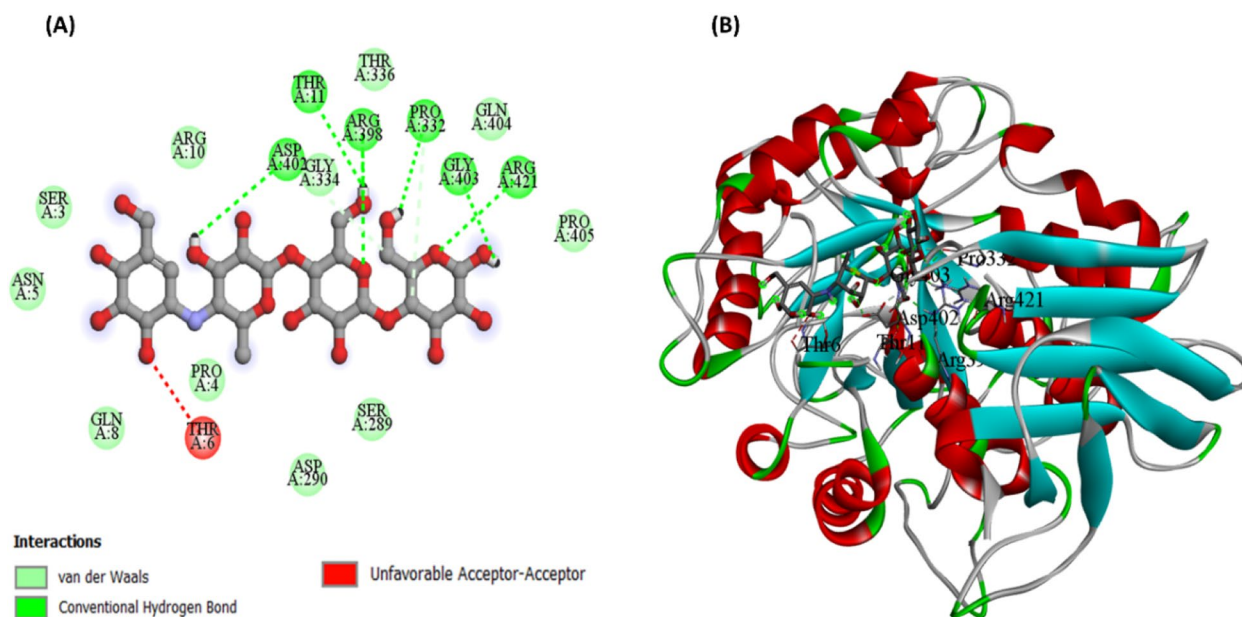


Fig. 6 Molecular docking of acarbose with α -amylase. **A** Two-dimensional representation of amino acid residues and various interaction involved in acarbose and α -amylase complex, **B** three-dimensional representation of binding of acarbose with α -amylase

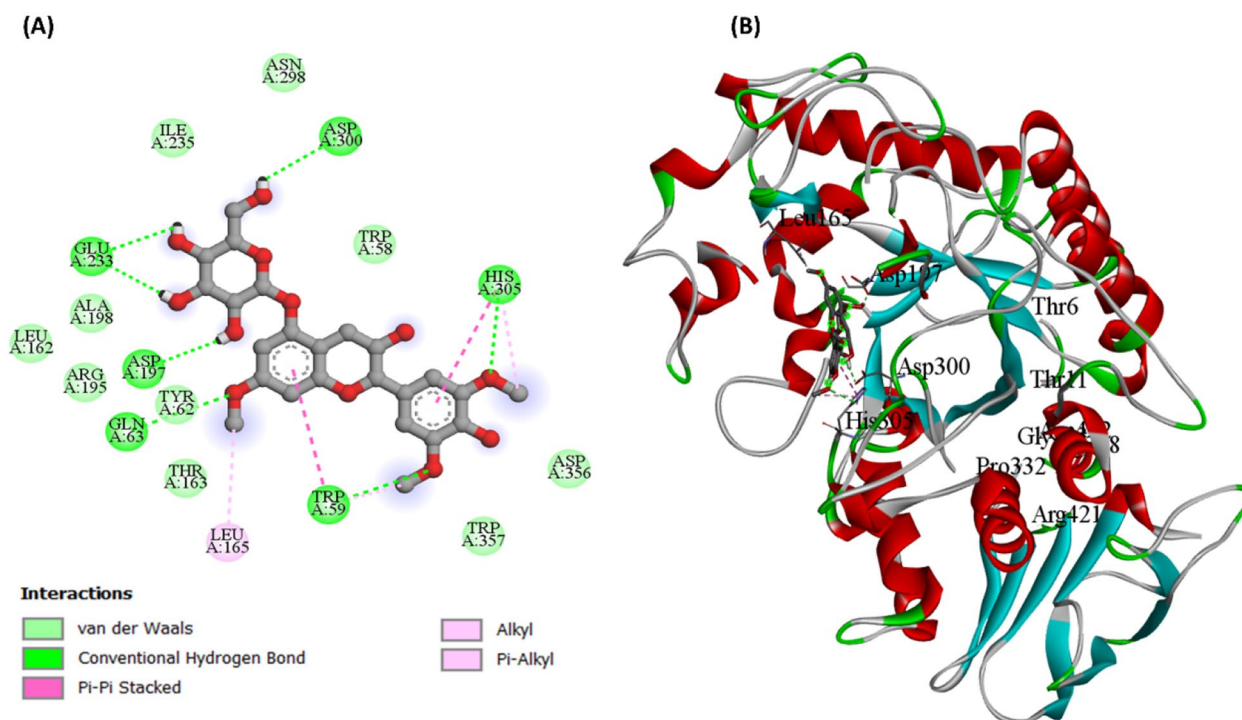


Fig. 7 Molecular docking of (3S,7E,9S)-9-Hydroxy-4,7-megastigmadien-3-one 9 glucoside with α -amylase. **A** Two-dimensional representation of amino acid residues and various interaction involved in (3S,7E,9S)-9-Hydroxy-4,7-megastigmadien-3-one 9 glucoside and α -amylase complex, **B** three-dimensional representation of binding of (3S,7E,9S)-9-hydroxy-4,7-megastigmadien-3-one 9 glucoside with α -amylase

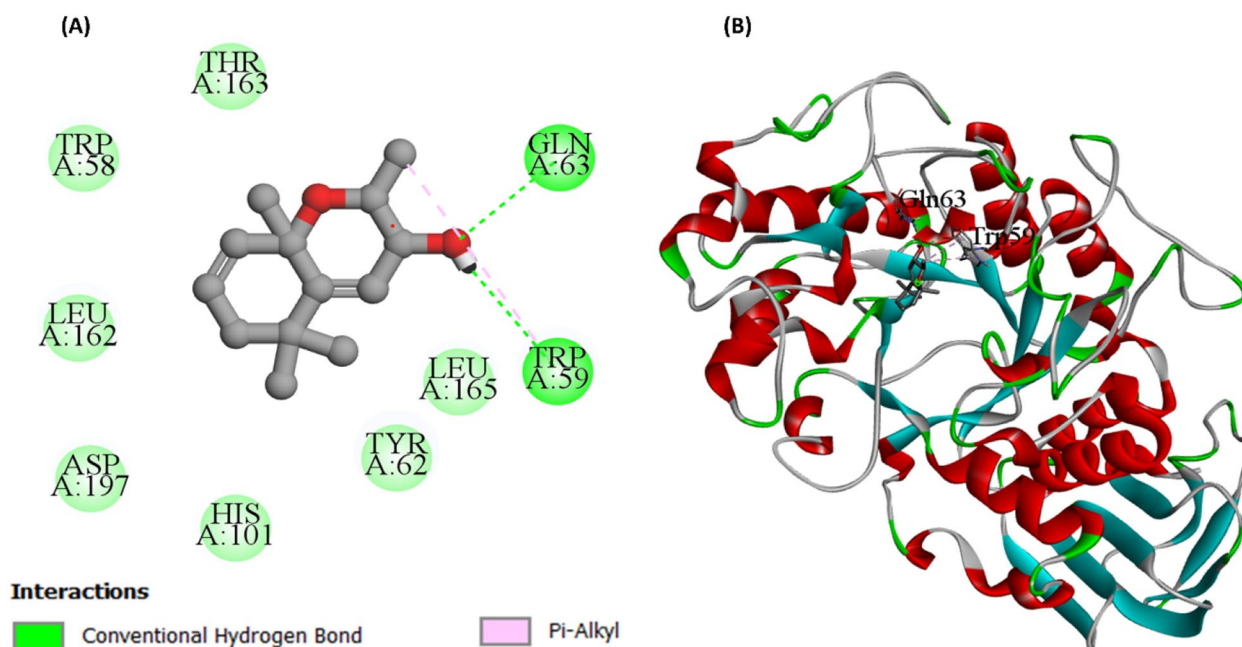


Fig. 8 Molecular docking of (5a,8b,9b)-5,9-Epoxy-3,6-megastigmadien-8-ol with α -amylase. **A** Two-dimensional representation of amino acid residues and various interaction involved in (5a,8b,9b)-5,9-Epoxy-3,6-megastigmadien-8-ol and α -amylase complex, **B** three-dimensional representation of binding of (5a,8b,9b)-5,9-Epoxy-3,6-megastigmadien-8-ol with α -amylase

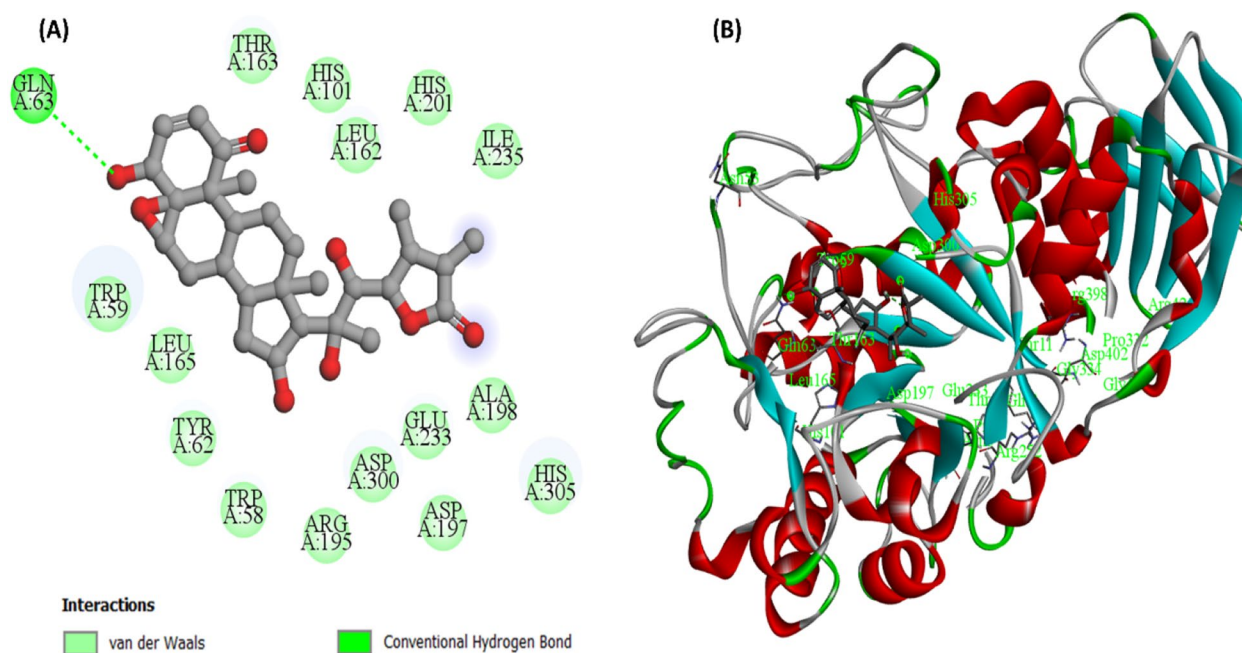


Fig. 9 Molecular docking of Ixocaralactone A with α -amylase. **A** Two-dimensional representation of amino acid residues and various interaction involved in Ixocaralactone A and α -amylase complex, **B** three-dimensional representation of binding of Ixocaralactone A with α -amylase

antimicrobial properties against the tested bacteria as compared to LSB. Regardless, gram-positive bacteria showed more resistance to both extracts when compared

to gram-negative bacteria. These results support the findings of Abdollahzadeh et al. [35], who documented the susceptibility of gram-negative bacteria to polyphenolic

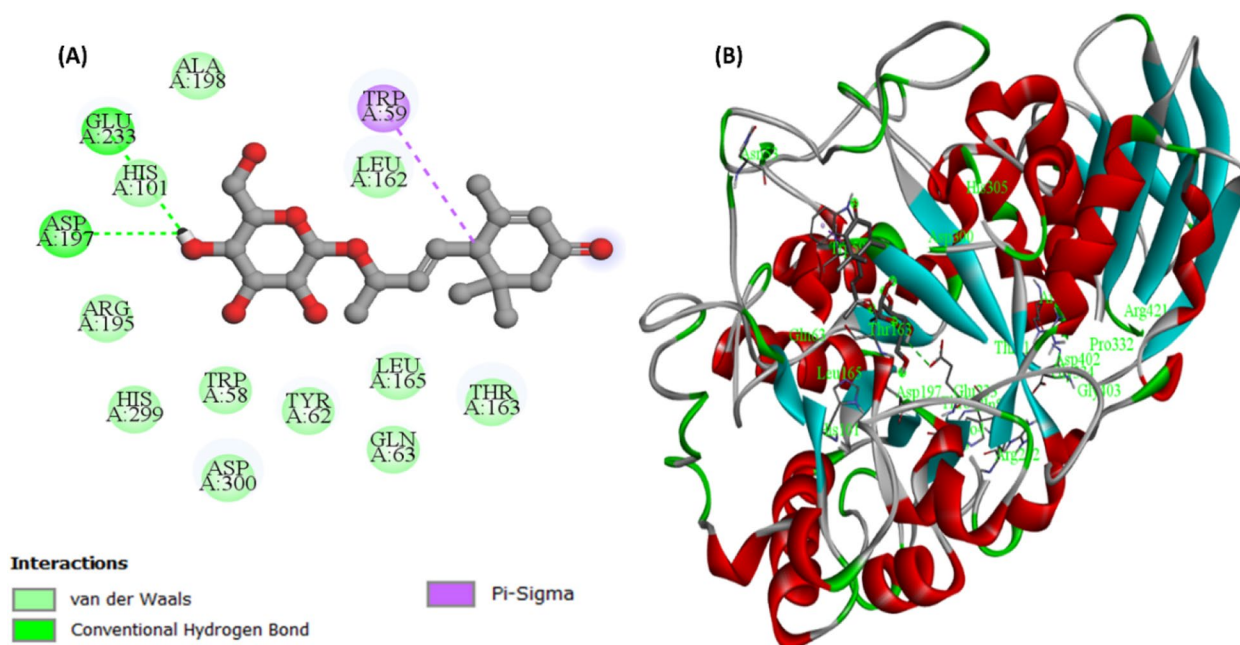


Fig. 10 Molecular docking of plumerubroside with α -amylase. **A** Two-dimensional representation of amino acid residues and various interaction involved in plumerubroside and α -amylase complex, **B** three-dimensional representation of binding of plumerubroside with α -amylase

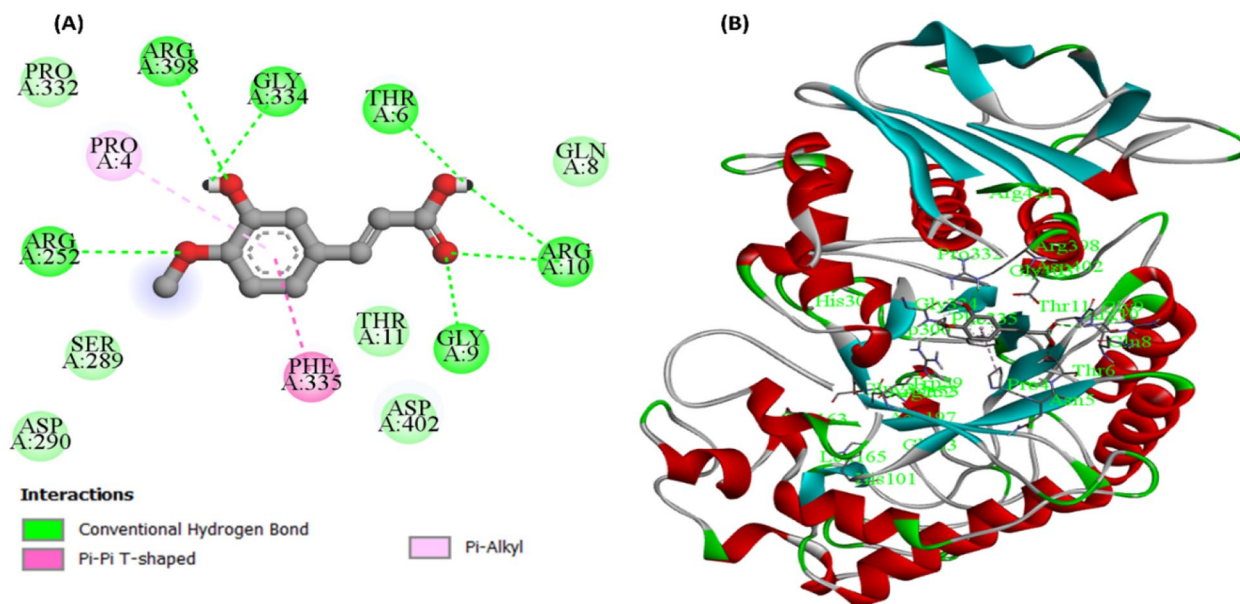


Fig. 11 Molecular docking of isoferulic acid with α -amylase. **A** Two-dimensional representation of amino acid residues and various interaction involved in isoferulic acid and α -amylase complex, **B** three-dimensional representation of binding of isoferulic acid with α -amylase

compounds due to their thin peptidoglycan cell wall in comparison with gram-positive bacteria. Therefore, the results from this study suggested that *B. strigosa* leaves showed antimicrobial effects against both gram-positive and gram-negative bacteria.

In vitro cell viability and nitrite productions

The effect of BSTR and LSB on cell viability was assessed on RAW 264.7 cells (Fig. 1). The results demonstrated that the treated RAW 264.6 cells were more than 80% viable at the tested concentrations (7.8–500 $\mu\text{g/mL}$).

However, both BSTR and LSB reduced the viability of RAW 264.7 cells at 1000 $\mu\text{g/mL}$. The IC_{50} values were $1034.44 \pm 0.96 \mu\text{g/mL}$ and $1312.93 \pm 1.71 \mu\text{g/mL}$ for BSTR and LSB, respectively, indicating good biocompatibility with the macrophages.

Meanwhile, inflammation is a physiological, self-limiting process occurring in mammalian tissues in response to harmful situations, such as microorganism invasion, physical damage, exposure to toxic chemicals or due to tissue stress and malfunction [36]. Macrophages are phagocytic, antigen-presenting, immunomodulatory cells that play critical roles in innate immune defense by secreting specific regulatory molecules [37].

Inflammatory processes tend to eliminate primary triggers and contribute to initiating the regeneration of injured tissues by mediating an organized immune response, involving macrophage cells [38]. Therefore, the inhibition of nitric oxide (NO), an inflammatory mediator from LPS-activated macrophages was investigated. The results indicated that treatment of cells with BSTR and LSB at 500 $\mu\text{g/mL}$ in the presence of LPS (50 ng/mL) showed significant reduction ($p < 0.001$) in NO secretion; however, elevated level of NO was not affected at concentrations of 3.9–31.2 $\mu\text{g/mL}$ (Fig. 2). BSTR ($\text{IC}_{50} = 186.07 \pm 1.96 \mu\text{g/mL}$) inhibited NO secretion by ~ 1.6 times more effectively than LSB

Table 5 Details of binding affinities and interaction of some selected compounds against α -amylase

Sr. No	Compound	Binding affinity (kcal/mol)	No. of H. Bonds	Interacting residues
1	Acarbose (standard)	-7.8	6	ASP A:402, THR A:11, ARG A:398, PRO A:332, GLY A:403, ARG A:421, THR A:6, ASN A:5, SER A:3, ARG A:10, THR A:336, GLN A:404, PRO A:405, GLN A:8, PRO A:4, ASP A:290, SER A:289
2	(3 <i>S</i> ,7 <i>E</i> ,9 <i>S</i>)-9-Hydroxy-4,7-megastigmadien-3-one 9-glucoside	-8.8	6	GLN A:63, ASP A:197, GLU A:233, ASP A:300, HIS A:305, THR A:163, LEU A:165, ILE A:235, ASN A:298, TRP A:58, ASP A:356, TRP A:357, THR A:163, TYR A:62, ARG A:195, LEU A:162, ALA A:198
3	(5 <i>a</i> ,8 <i>b</i> ,9 <i>b</i>)-5,9-Epoxy-3,6-megastigma	-6.6	2	GLN A:63, TRP A:59, LEU A:165, TYR A:62, HIS A:101, ASP A:197, LEU A:162, TRP A:58, THR A:163
4	Ixocarpalactone A	-9.5	1	GLN A:63, THR A:163, HIS A:101, LEU A:162, HIS A:201, ILE A:235, TRP A:59, LEU A:165, TYR A:62, TRP A:58, ARG A:195, ASP A:300, GLY A:233, ALA A:198, ASP A:197, HIS A:305
5	Plumerubroside	-8.1	2	ASP A:197, TRP A:59, ALA A:198, HIS A:101, ARG A:195, HIS A:299, TRP A:58, ASP A:300, TYR A:62, LEU A:165, GLN A:63, THR A:163, LEU A:162
6	Isoferulic acid	-6.1	6	ARG A:252, ARG A:398, GLY A:334, THR A:6, ARG A:10, GLY A:9, PRO A:4, PHE A:335, PRO A:332, GLN A:8, THR A:11, ASP A:402, SER A:289, ASP A:290, SER A:289

Table 6 Details of binding affinity and interaction of some selected compounds with α -glucosidase

Sr. No	Compound	Binding affinity (kcal/mole)	No. of H. Bonds	Interacting residues
1	Acarbose (standard)	-7.1	7	PRO A:433, MET A:435, LYS A:436, ASP A:379, ASP A:381, VAL A:383, ASP A:382, ASP A:59, ASN A:58, ASN A:61, ARG A:17, ILE A:27, TRP A:434
2	(3 <i>S</i> ,7 <i>E</i> ,9 <i>S</i>)-9-Hydroxy-4,7-megastigmadien-3-one 9-glucoside	-8.1	4	GLU A:119, LYS A:118, GLU A:157, ARG A:123, TRP A:128, ASP A:124, TYR A:126, ILE A:204, ASN A:171, TRP A:172, LYS A:206, GLU A:173, ILE A:127, ALA A:208, PHE A:210, HIS A:129
3	(5 <i>a</i> ,8 <i>b</i> ,9 <i>b</i>)-5,9-Epoxy-3,6-megastigma	-6.1	N/A	GLY A:274, TRP A:6, ASN A:277, ALA A:247, ILE A:251, PHE A:246, LYS A:242, THR A:253, ASN A:245, PHE A:276
4	Ixocarpalactone A	-7.9	2	GLU A:283, GLY A:286, GLY A:259, PRO A:233, LEU A:219, PRO A:216, PRO A:214, VAL A:222, GLU A:226, PHE A:225, MET A:229, ASN A:258, PHE A:282, LEU A:287
5	Plumerubroside	-7.7	3	ASN A:227, ASN A:275, PHE A:276, LYS A:242, GLY A:274, GLU A:271, LYS A:7, TRP A:6, ALA A:247, TYR A:249, ASP A:250, ILE A:251, MET A:252, PHE A:246
6	Isoferulic acid	-5.9	3	ASN A:316, GLY A:317, TRP A:318, ALA A:270, TRP A:6, VAL A:269, ASN A:277, PHE A:276, ASN A:275, GLY A:274, LYS A:242, GLU A:271, LYS A:7

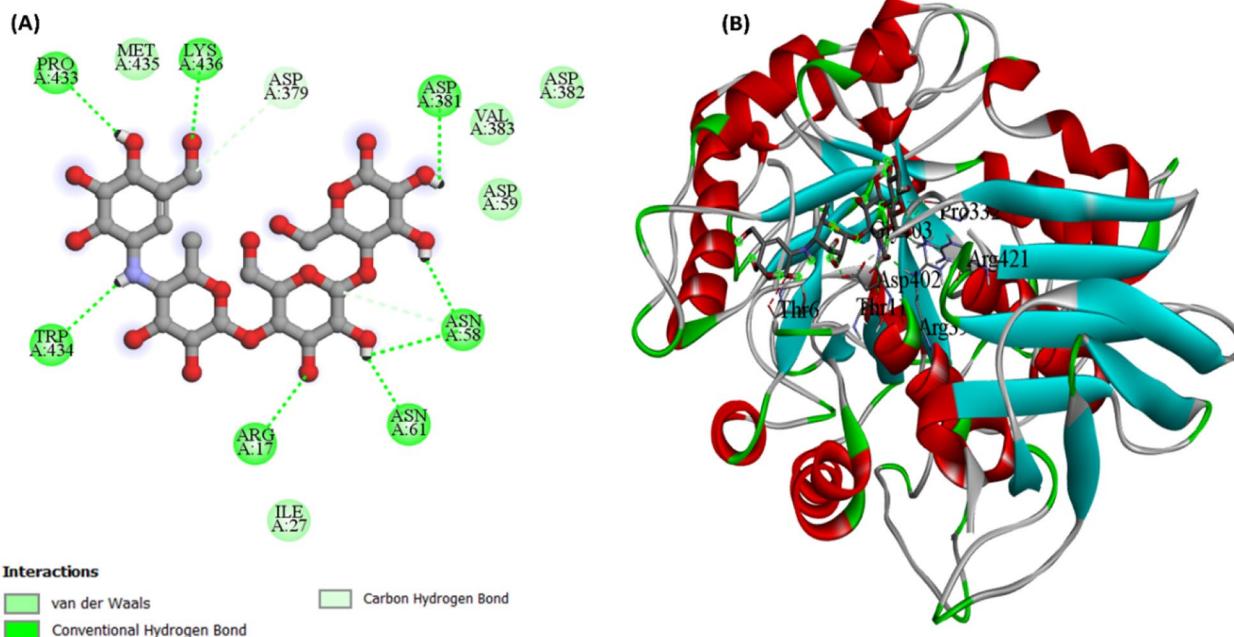


Fig. 12 Molecular docking of acarbose with α -glucosidase. **A** Two-dimensional representation of amino acid residues and various interaction involved in acarbose and α -glucosidase complex, **B** three-dimensional representation of binding of acarbose with α -glucosidase

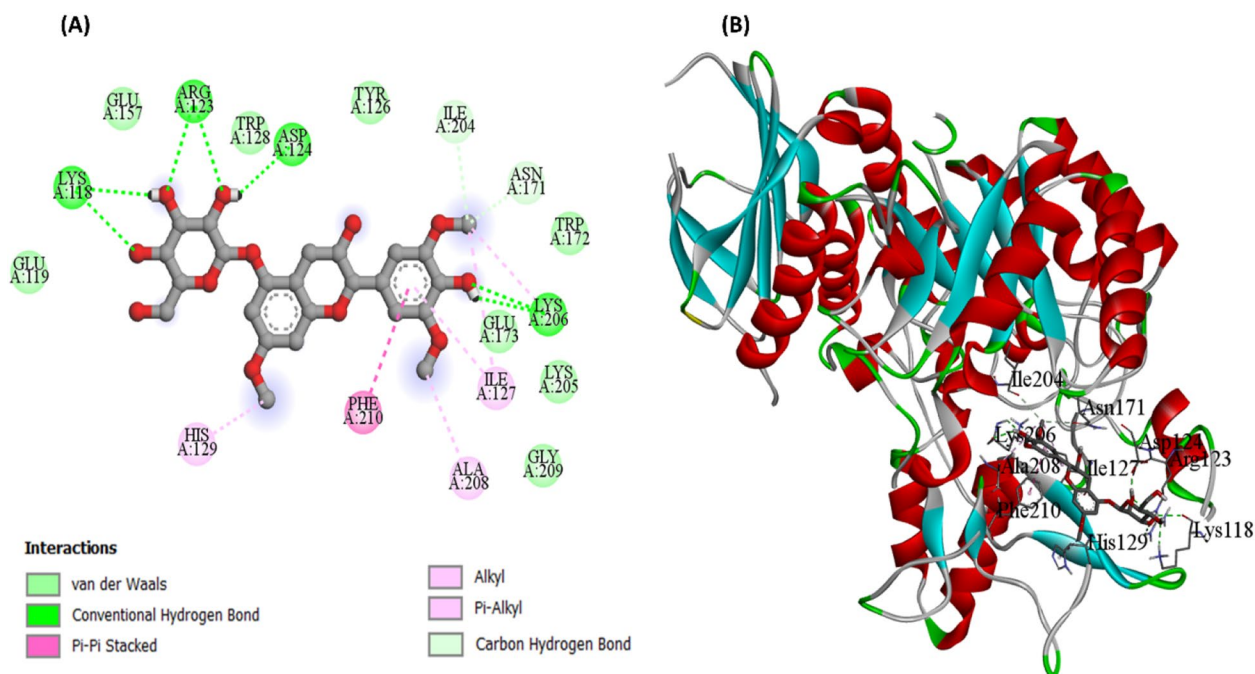


Fig. 13 Molecular docking of (3S,7E,9S)-9-Hydroxy-4,7-megastigmadien-3-one 9 glucoside with α -glucosidase. **A** Two-dimensional representation of amino acid residues and various interaction involved in (3S,7E,9S)-9-Hydroxy-4,7-megastigmadien-3-one 9 glucoside and α -glucosidase complex, **B** three-dimensional representation of binding of (3S,7E,9S)-9-Hydroxy-4,7-megastigmadien-3-one 9 glucoside with α -glucosidase

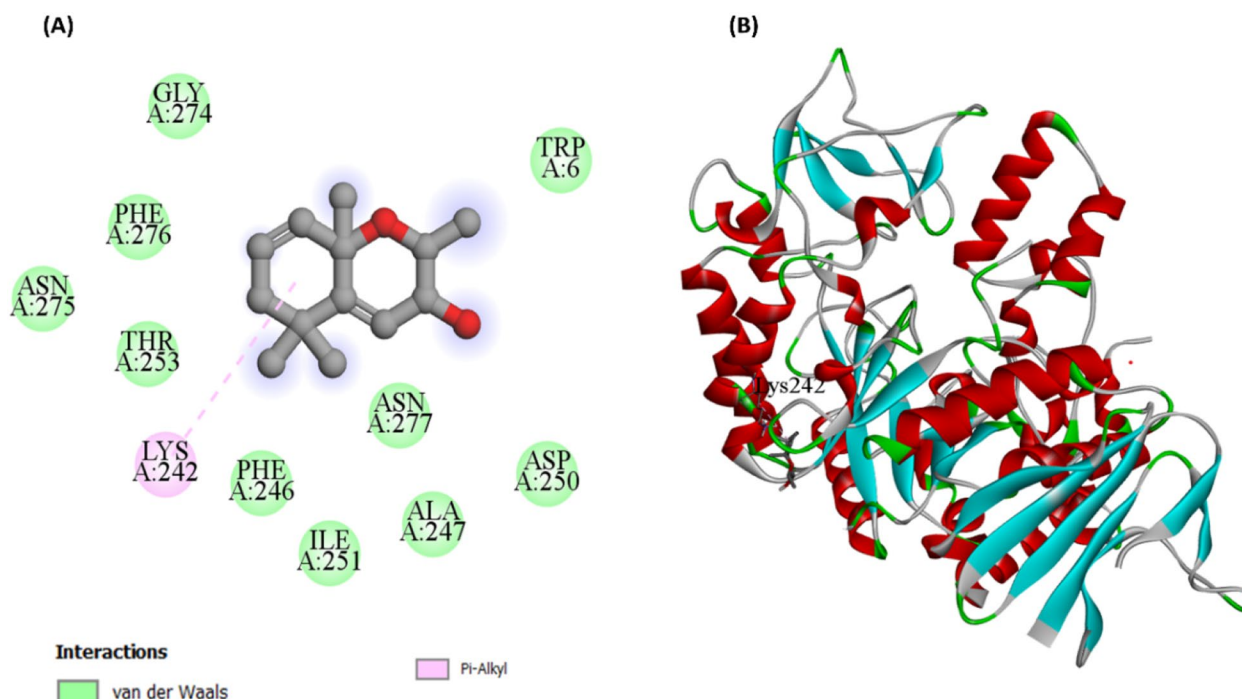


Fig. 14 Molecular docking of (5a,8b,9b)-5,9-Epoxy-3,6-megastigmadien-8-ol with α -glucosidase. **A** Two-dimensional representation of amino acid residues and various interaction involved in (5a,8b,9b)-5,9-Epoxy-3,6-megastigmadien-8-ol and α -glucosidase complex, **B** three-dimensional representation of binding of (5a,8b,9b)-5,9-Epoxy-3,6-megastigmadien-8-ol with α -glucosidase

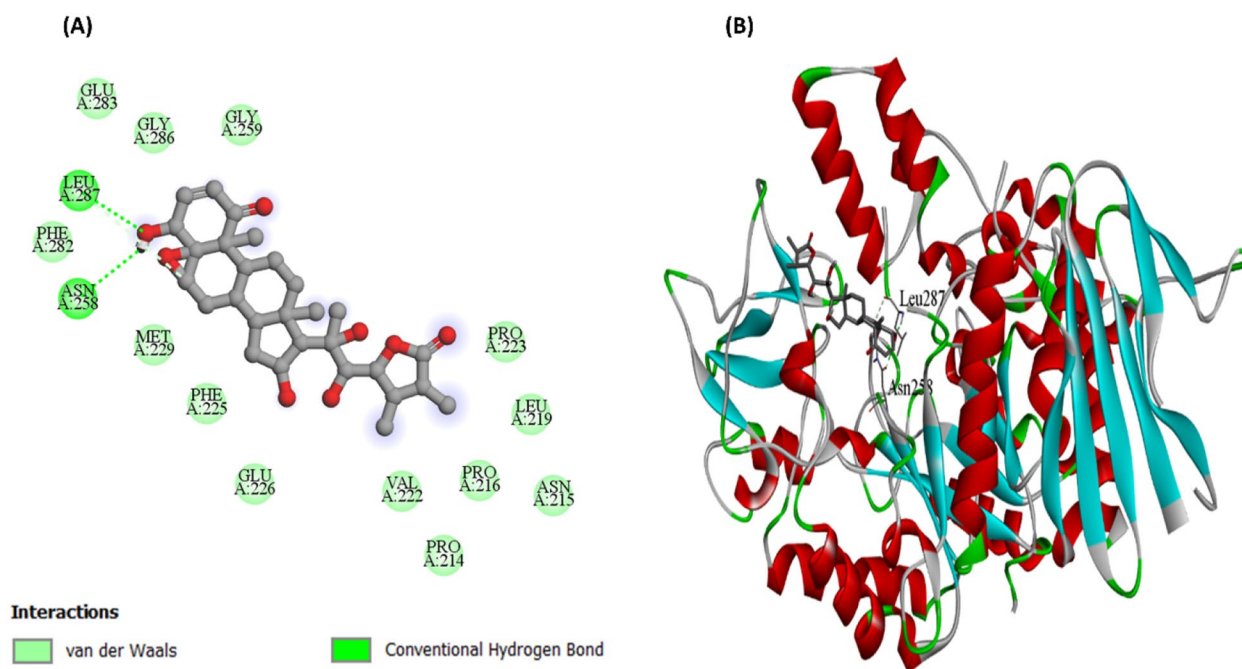


Fig. 15 Molecular docking of ixocarpalactone A with α -glucosidase. **A** Two-dimensional representation of amino acid residues and various interaction involved in Ixocarpalactone A and α -glucosidase complex, **B** three-dimensional representation of binding of ixocarpalactone A

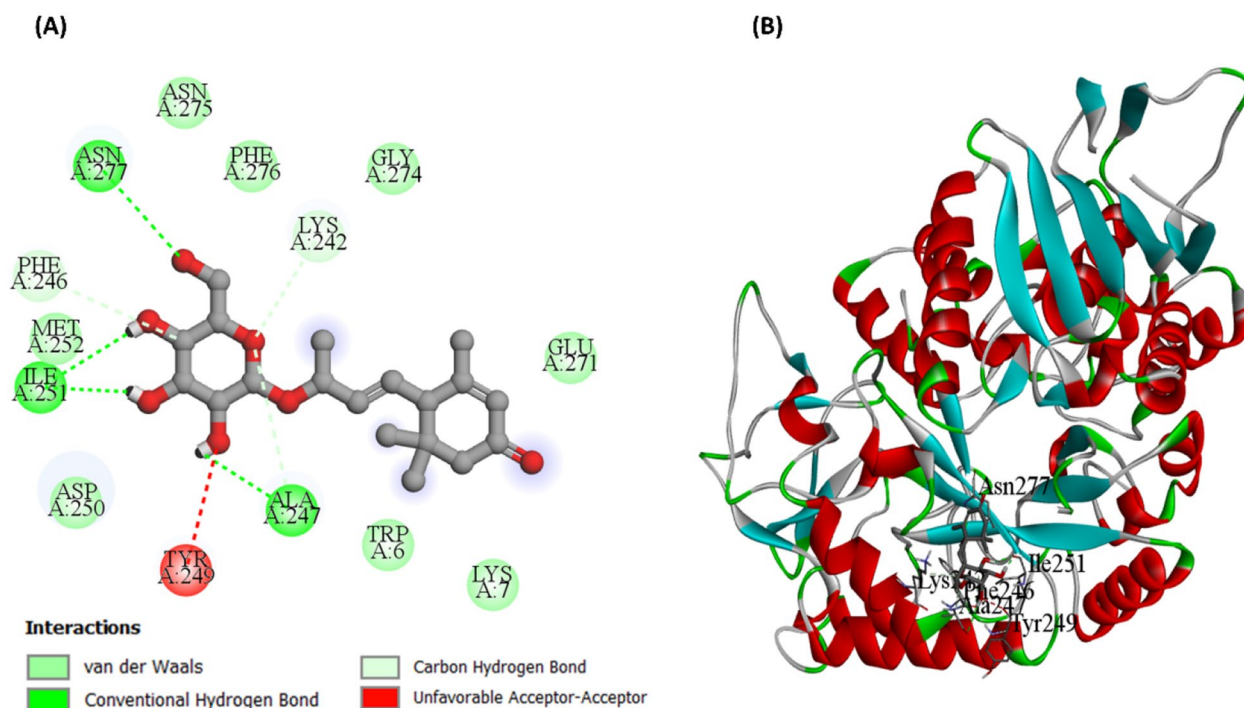


Fig. 16 Molecular docking of plumerubroside with α -glucosidase. **A** Two-dimensional representation of amino acid residues and various interaction involved in plumerubroside and α -glucosidase complex, **B** three-dimensional representation of binding of plumerubroside

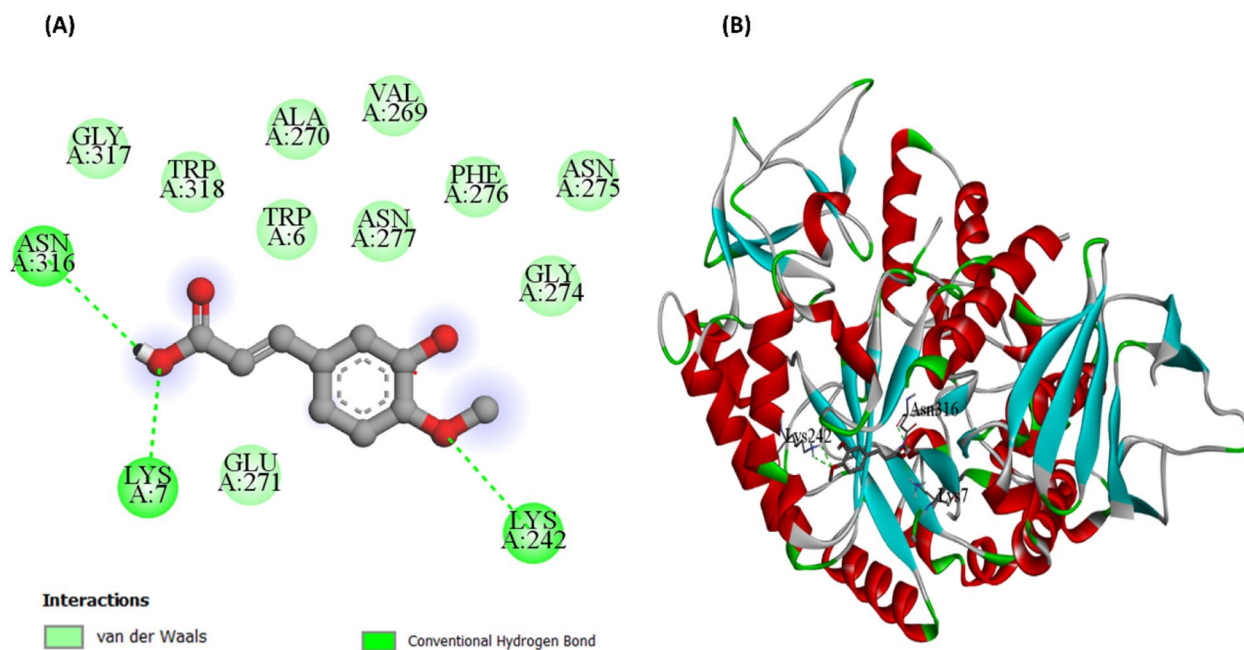


Fig. 17 Molecular docking of isoferulic acid with α -glucosidase. **A** Two-dimensional representation of amino acid residues and various interaction involved in isoferulic acid and α -glucosidase complex, **B** three-dimensional representation of binding of isoferulic acid α -glucosidase

Table 7 Details of physicochemical parameters evaluated through in silico studies

Sr No	Compound	Physicochemical properties						Water solubility		
		Hydrogen bond donor	Hydrogen bond acceptor	Molecular weight g/mol	Lipophilicity	Molar refractivity	Lipinski violation	Class		
								ESOL	Ali	Silicos-IT
1	(3S,7E,9S)-9-Hydroxy-4,7-megastigmadien-3-one 9-glucoside	4	7	370.44	2.31	95.03	0	Very soluble	Soluble	Soluble
2	(5a,8b,9b)-5,9-Epoxy-3,6-megastigma	1	2	208.30	2.25	61.45	0	Soluble	Soluble	Soluble
3	Ixocarpalactone A	4	8	504.61	2.86	130.33	1	Moderately soluble	Moderately soluble	Soluble
4	Plumerubroside	6	12	510.49	3.03	121.89	3	Soluble	Soluble	Soluble
5	Isoferulic acid	2	4	194.18	1.79	51.63	0	Soluble	Soluble	Soluble

($IC_{50} = 305.207 \pm 0.92$ $\mu\text{g/mL}$) with selectivity index (SI) of 5.5 and 4.3, respectively, indicating the potency of BSTR when compared to LSB. Among the tested extract at non-toxic doses, BSTR showed a dose-dependent reduction in NO secretion. Moreover, the viability of LPS-stimulated cells was not affected by BSTR and LSB at the tested concentrations (3.9–500 $\mu\text{g/mL}$) (Fig. 2). These results indicated that the phyto-constituents such as polyphenols, terpenoids, diterpenes, and sesquiterpenes in the extracts might have potential anti-inflammatory effects by reducing the secretion of inflammatory cytokines.

Antiproliferative activity

The cytotoxic activity of BSTR and LSB was analyzed against CLS-354/WT cancer cell line. As shown in Fig. 3, a concentration dependent cytotoxic effect was displayed by both extracts. BSTR exhibited 90% cytotoxicity against CLS-354/WT cells from 400 to 1600 $\mu\text{g/mL}$. Moreover, BSTR ($CC_{50} = 234.23 \pm 0.49$) inhibited CLS-354/WT cell viability by approximately 0.95 times when compared to LSB ($CC_{50} = 312.50 \pm 0.92$) with SI of 4.4 and 4.2, respectively, indicating the potency of BSTR compared to LSB. Furthermore, BSTR and LSB significantly ($p < 0.001$) inhibited the proliferation of cells with cellular apoptosis. These results suggested that BSTR and LSB have pronounced anti-proliferative effect on CLS-354/WT via apoptosis rather than necrosis approach. In addition, both extracts significantly inhibited cell migration (Figs. 3 and 4). Cancer is one of the most prevailing disease in humans and the high morbidity and mortality rates associated with cancer has necessitated urgent need for effective treatment. Numerous plants have been evaluated for their anticancer, antitumor and antiproliferative properties [5, 39, 40]. Previous studies have reported the antiproliferative activities of extracts and bioactive compounds identified from some *Barleria* species. According to El-Halawany et al. verbascoside, isoverbascoside, dimethoxyverbascoside, hydroxybenzoic acid and apigenin-7-O-glucoside isolated from *Barleria cristata* showed cytotoxic effect against Hepa-1c1c7 cells at a concentration of 3.125 μM [39]. Similarly, Manglani et al. [41] reported the anticancer efficacy of *Barleria grandiflora* leaves extract against human lung cancer cells (A-549) and Dalton's lymphoma ascites (DLA tumor) cells at IC_{50} values of 143.4 and 137.2 $\mu\text{g/mL}$, respectively. It is noteworthy that the occurrence of several bioactive constituents with reported anticancer efficacy in *B. strigosa* suggested that the potent cytotoxic and antiproliferative effect might be associated with the combined synergistic effects of these compounds.

Cellular apoptosis by nuclear staining

The nuclei of healthy cells are generally spherical, with evenly distributed DNA; however, during cellular apoptosis, the DNA of cells are condensed. Therefore, nuclear condensation is generally used for distinguishing between healthy and apoptotic or necrotic cells. Apoptosis, a genetically programmed cellular event leads to biochemical and morphological changes in the cells. Alterations in DNA caused by several factors can affect the nucleus and ultimately the entire cell leading to compromised function of the organ and organism [42]. The morphological changes in BSTR and LSB treated CLS-354/WT cells were observed after 24 h using DAPI nucleus staining. As shown in Fig. 5, the fluorescent results indicated normal spherical nuclei, with blue, pale chromatin and organized structure for the untreated cells. However, condensed chromatin with fragmented nuclei were observed after exposure of the cells to BSTR and LSB extracts. These results suggested that BSTR and LSB showed anticancer effects with cellular apoptosis [5, 21].

In silico molecular docking studies

Computational analysis, particularly *in-silico* molecular docking is a reliable and accurate tool for predicting the interaction of ligands with target molecules, their binding energy, underlying mechanisms and correlating the biological activities of therapeutic plants observed in the experiments on a molecular basis [43]. The compounds from the UPLC-QTOF-ESI-MS profile along with standard acarbose were docked with α -amylase and α -glucosidase (Figs. 6, 7, 8, 9, 10 and 11). The inhibition of enzymes was mainly attributed to the formation of Van der Waals, hydrogen bond, pi-alkyl, alkyl, and pi-sigma interactions at the active sites of the enzymes. Compounds such as (3*S*,7*E*,9*S*)-9-hydroxy-4,7-megastigmadien-3-one 9-glucoside is surrounded by amino acid residues such as ASP A300, TRP A59, ASP A197, HIS A305 and GLU A233 which constitute the active site of α -amylase [44] as shown in Fig. 7. Similarly, isoferulic acid was observed with six conventional hydrogen bonding with amino acid residues of α -amylase including ARG A:398, GLY A:334, ARG A:10, GLY A:9 and ARG A:252 (Fig. 11). All these amino acid residues are reported to constitute the active pockets of the enzyme [45]. Moreover, ixocarpalactone A and plumerubroside showed lower binding energy against α -amylase as compared to the standard acarbose (Table 5). This might be due to the presence pi bonding (Fig. 7).

For the α -glucosidase enzyme, (3*S*,7*E*,9*S*)-9-hydroxy-4,7-megastigmadien-3-one 9-glucoside was observed with the highest binding affinity of -8.1 kcal/mol, higher than the binding affinity of the standard acarbose (Table 6). The compound was surrounded by amino

Table 8 Details of physicochemical parameters evaluated through in silico studies

Sr No	Compounds	GI absorption	BBB Permeant	P-glycoprotein substrate	CYP inhibitors				Log Kp skin permeation (cm/s)
					CYP 1A2	CYP 2C19	CYP 2C9	CYP 2D6	
1	(3S,7E,9S)-9-Hydroxy-4,7-megastigmadien-3-one 9-glucoside	High	No	Yes	No	No	No	Yes	-8.54
2	(5a,8b,9b)-5,9-Epoxy-3,6-megastigma	High	Yes	No	No	No	No	No	-6.25
3	Ixocarpalactone A	High	No	Yes	No	No	No	No	-7.88
4	Plumerubroside	Low	No	Yes	No	No	No	No	-9.24
5	Isoferulic acid	Low	Yes	No	No	No	No	No	-6.41

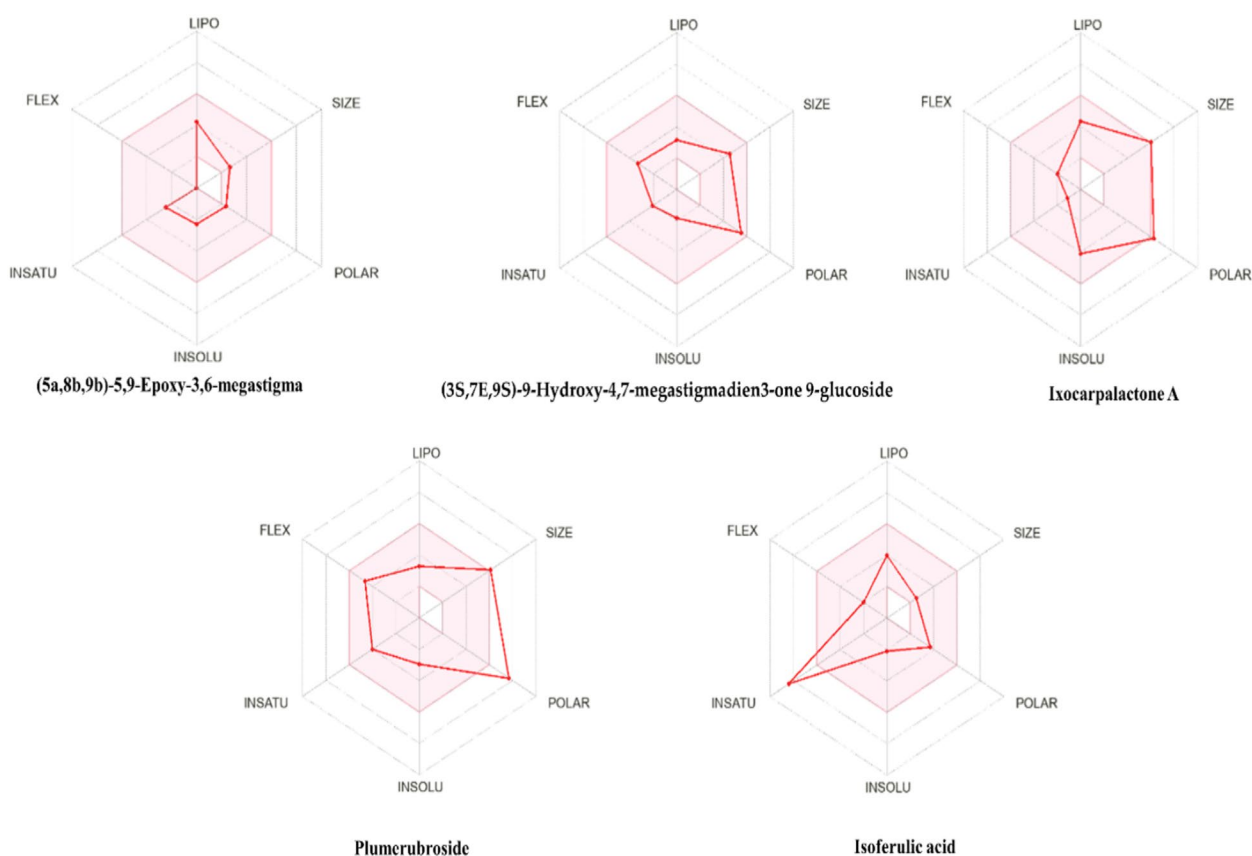


Fig. 18 Bioavailability radar

acid residues such as LYS A:436, ASP A:381, ASN A:58, ASN A:61, ARG A:17, TRP A:434 and PRO A:433 forming conventional hydrogen bonding with active site of the enzyme [45]. The other compounds ixocarpalactone A and plumerubroside showed good binding affinity for the protein when compared to the standard (Table 6 and Figs. 12, 13, 14, 15, 16 and 17). The variation in the bonding of the ligands with proteins results in the difference of binding affinity [46].

To determine the drug-likeness, physiochemical properties, and pharmacodynamics of the compounds, the

SwissADME was used [47]. ADME properties provide insights on whether the molecules under study can be used as future medicines or not [48]. Compounds having lower molecular weight, lipophilicity, and lower hydrogen bond capacity possess good absorption, high bioavailability, and distribution [49, 50]. If a chemical compound follows all the criteria of Lipinski's rule it shows a drug-like behavior and it is considered as a potential therapeutic agent. On the other hand, if a chemical compound fails to follow more than one Lipinski's criteria it is considered an orally unavailable drug. Lipinski's rule has the following five criteria: (1) molecular

Table 9 In silico evaluation of the toxicity profile of the selected compounds

Sr No	Compound	LD50 (mg/kg)	Predicted class	Hepatotoxic	Carcinogenic	Immunotoxic	Mutagenic	Cytotoxic
1	(3S,7E,9S)-9-Hydroxy-4,7-megastigmadien-3-one 9-glucoside	4500	4	Inactive	Inactive	Inactive	Inactive	Inactive
2	(5a,8b,9b)-5,9-Epoxy-3,6-megastigma	1190	4	Active	Inactive	Active	Inactive	Inactive
3	Ixocarpalactone A	25	2	Inactive	Inactive	Active	Inactive	Active
4	Plumerubroside	10000	6	Inactive	Inactive	Active	Inactive	Active
5	Isoferulic acid	7900	6	Inactive	Inactive	Active	Inactive	Inactive

weight (less than 500); (2) lipophilicity (Log P o/w less than 5); (3) molecular refractivity (40–130); (4) hydrogen bond acceptor (≤ 10); hydrogen bond donor (less than equal to 5) [51]. All the docked compounds except for plumerubroside showed one or less than one violation, suggesting that all the compounds are orally bioavailable drugs (Tables 7 and 8, Fig. 18). Plumerubroside showed 3 violations which predicted it is orally inactive and unstable. To predict toxicity, the PROTOX-II program makes use of the chemical structure and compares it with other chemical compounds with known toxicity [52]. The results of in silico toxicity analysis showed that all the analyzed compounds have low toxic potentials with no mutagenicity calculated for any of the compounds (Table 9).

Conclusion

This study revealed that the extract from the leaves of *B. strigosa* is a rich plethora of bioactive constituents, majorly terpenoids and polyphenolic compounds which were putatively identified by LC–MS analysis. Furthermore, *B. strigosa* exhibited excellent antioxidant, antidiabetic, anti-inflammatory, antiproliferative and antibacterial properties, thus shedding scientific light to the pharmacological activities of *B. strigosa*. Overall, these results pave the way for further investigations on the prospects of this plant in combating oxidative induced disorders.

Acknowledgements

The authors are grateful to the Scientific Research Fund for Key Projects of Wannan Medical College (grant number WK2021ZF03) for the financial support.

Author contributions

Conceptualization: ML and OJO; data curation: LW, CO; formal analysis: OOO, ML, LW, and SS; fund acquisition: ML; investigation: OOO, ML, LW, AB, SS CO and OJO; methodology: OJO, and SS; supervision: ML; OJO; writing—original draft, OOO, OJO, SS, and AS; writing—review and editing: OJO. All authors have read and agreed to the published version of the manuscript.

Funding

The authors are grateful to the Scientific Research Fund for Key Projects of Wannan Medical College (Grant Number WK2021ZF03) for the financial support.

Availability of data and materials

Data will be made available on request from the corresponding author.

Declarations

Ethics approval and consent to participate

Not applicable.

Consent for publication

Not applicable.

Competing interests

The authors declare no conflict of interest with respect to the work described in this manuscript.

Author details

¹Department of Pharmacy, The First Affiliated Hospital of Wannan Medical College, Wuhu 241000, China. ²Department of Food and Human Nutritional Sciences, Faculty of Agricultural and Food Sciences, University of Manitoba, Winnipeg, MB R3T 2N2, Canada. ³Department of Pharmaceutical Sciences, Faculty of Pharmacy, Chiang Mai University, Chiang Mai 50200, Thailand. ⁴Department of Pharmaceutical Chemistry, Faculty of Pharmaceutical Sciences, Prince of Songkla University, Hat Yai 90112, Thailand. ⁵Drug Delivery System Research Excellence Center, Faculty of Pharmaceutical Sciences, Prince of Songkla University, Hat Yai 90112, Thailand. ⁶African Genome Center, Mohammed VI Polytechnic University, 43150 Ben Guerir, Morocco.

Received: 10 June 2023 Accepted: 29 July 2023

Published: 7 August 2023

References

- Lahlou M. The success of natural products in drug discovery. *Pharmacol Pharm.* 2013;4:17–31.
- Cragg GM, Newman DJ. Natural products: a continuing source of novel drug leads. *Biochim Biophys Acta.* 2013;1830:3670–95.
- Uysal S, Sinan KI, Jekó J, Cziáky Z, Zengin G. Chemical characterization, comprehensive antioxidant capacity, and enzyme inhibitory potential of leaves from *Pistacia terebinthus* L. (Anacardiaceae). *Food Biosci.* 2022;48:101820.
- Ekor M. The growing use of herbal medicines: Issues relating to adverse reactions and challenges in monitoring safety. *Front Pharmacol.* 2014;10:4–177.
- Olatunji OJ, Olatunde OO, Jayeoye TJ, Singh S, Nalinbenjapun S, Sripetthong S, Chunglok W, Ovatlarnporn C. New insights on *Acanthus ebracteatus* Vahl: UPLC-ESI-QTOF-MS profile, antioxidant, antimicrobial and anticancer activities. *Molecules.* 2022;27:1981.
- Shao H, Xiao M, Zha Z, Olatunji OJ. UHPLC-ESI-QTOF-MS² analysis of *Acacia pennata* extract and its effects on glycemic indices, lipid profile, pancreatic and hepatorenal alterations in nicotinamide/streptozotocin-induced diabetic rats. *Food Sci Nutr.* 2022;10:1058–69.
- Zengin G, Dall'Acqua S, Sinan KI, Uba AI, Sut S, Peron G, Etienne OK, Kumar M, Cespedes-Acuña CL, Alarcon-Enos J, Mollica A, Mahomoodally MF. Gathering scientific evidence for a new bioactive natural ingredient: The combination between chemical profiles and biological activities of *Flueggea virosa* extracts. *Food Biosci.* 2022;49:101967.
- Kanchanapoom T, Noiarsa P, Ruchirawat S, Kasai R, Otsuka H. Phenylethanoid and iridoid glycosides from the Thai medicinal plant. *Barleria strigosa* Chem Pharm Bull. 2004;52:612–4.
- Prapalert W, Santiarworn D, Liawruangrath S, Liawruangrath B, Pyne SG. Two phenylethanoid glycosides, parvifloroside A and B, isolated from *Barleria strigosa*. *Chiang Mai J Sci.* 2017;44:168–75.
- Manapradit N, Poearim S, Charoenying P. Cytotoxicity and antimicrobial activities of leaf extracts from *Barleria strigosa*. *Int J Agric Technol.* 2015;11:551–61.
- Deepak M, Sulaiman C, Balachandran I, Chandran KPS. Identification of medicinally active flavonoids, phenolic compounds and terpenoids from traditional healing plant *Barleria strigosa* and its antioxidant activity. *Asian J Green Chem.* 2021;5:12–22.
- Gangaram S, Naidoo Y, Dewir YH, El-Hendawy S. Phytochemicals and biological activities of *Barleria* (Acanthaceae). *Plants.* 2022;11:82.
- Huang Y, An M, Fang A, Olatunji OJ, Eze FN. Antiproliferative activities of the lipophilic fraction of *Eucalyptus camaldulensis* against MCF-7 breast cancer cells, UPLC-ESI-QTOF-MS metabolite profile, and antioxidative functions. *ACS Omega.* 2022;7:27369–81.
- Olatunde OO, Tan SLD, Shiekh KA, Benjakul S, Nirmal NP. Ethanolic guava leaf extracts with different chlorophyll removal processes: anti-melanosis, antibacterial properties and the impact on qualities of Pacific white shrimp during refrigerated storage. *Food Chem.* 2021;341:128251.
- Olatunde OO, Benjakul S, Huda N, Zhang B, Deng S. Ethanolic Noni (*Morinda citrifolia* L.) leaf extract dechlorophyllized using sedimentation process: antioxidant, antibacterial properties and efficacy in extending the shelf-life of striped catfish slices. *Int J Food Sci Technol.* 2020;56:2804–19.

16. Olatunde OO, Benjakul S, Vongkamjan K. Antioxidant and antibacterial properties of guava leaf extracts as affected by solvents used for prior dechlorophyllization. *J Food Biochem*. 2018;42:e12600.
17. Olatunde OO, Benjakul S, Vongkamjan K, Amnuait T. Liposomal encapsulated ethanolic coconut husk extract: antioxidant and antibacterial properties. *J Food Sci*. 2019;84:3664–73.
18. Kumar S, Kumar V, Prakash O. Enzymes inhibition and antidiabetic effect of isolated constituents from *Dillenia indica*. *Biomed Res Int*. 2013;2013:382063.
19. Makinde EA, Ovatlarnporn C, Adekoya AE, Nwabor OF, Olatunji OJ. Antidiabetic, antioxidant and antimicrobial activity of the aerial part of *Tiliacora triandra*. *S Afr J Bot*. 2019;125:337–43.
20. Odedina GF, Vongkamjan K, Voravuthikunchai SP. Potential bio-control agent from *Rhodomyrtus tomentosa* against *Listeria monocytogenes*. *Nutrients*. 2015;7:7451–68.
21. Singh S, Chidrawar VR, Hermawan D, Nwabor OF, Olatunde OO, Jayeoye TJ, Samee W, Ontong JC, Chittasupho C. Solvent-assisted dechlorophyllization of *Psidium guajava* leaf extract: effects on the polyphenol content, cytocompatibility, antibacterial, anti-inflammatory, and anticancer activities. *S Afr J Bot*. 2023;158:166–79.
22. Basit A, Ahmad S, Khan K-u-R, Aati HY, Sherif AE, Ovatlarnporn C, Khan S, Rao H, Arshad MA, Shahzad MN. Evaluation of anti-inflammatory, antioxidant and cytotoxic potential of *Cardamine amara* L. (Brassicaceae): a comprehensive biochemical, toxicological and in silico computational study. *Front Chem*. 2023;10:1577.
23. Dilshad R, Ahmad S, Aati HY, Al-Qahtani JH, Sherif AE, Hussain M, Ghalloo BA, Tahir H, Basit A, Ahmed M. Phytochemical profiling, *in vitro* biological activities, and in-silico molecular docking studies of b. Arabian J Chem. 2022;15:104133.
24. Daina A, Michielin O, Zoete V. SwissADME: a free web tool to evaluate pharmacokinetics, drug-likeness and medicinal chemistry friendliness of small molecules. *Sci Rep*. 2017;7:42717.
25. Wen C, Liu C, Li Y, Xia T, Zhang X, Xue S, Olatunji OJ. Ameliorative potentials of the ethanolic extract from *Lycium chinense* leaf extract against diabetic cardiomyopathy. Insight into oxido-inflammatory and apoptosis modulation. *Biomed Pharmacother*. 2022;154:113583.
26. Olatunji OJ, Chen H, Zhou Y. Neuroprotective effect of trans-N-caffeoyl-tyramine from *Lycium chinense* against H₂O₂ induced cytotoxicity in PC12 cells by attenuating oxidative stress. *Biomed Pharmacother*. 2017;93:895–902.
27. Makinde EA, Radenahmad N, Adekoya AE, Olatunji OJ. *Tiliacora triandra* extract possesses antidiabetic effects in high fat diet/streptozotocin-induced diabetes in rats. *J Food Biochem*. 2020;44:e13239.
28. Olatunji OJ, Zuo J, Olatunde OO. *Securidaca inappendiculata* stem extract confers robust antioxidant and antidiabetic effects against high fructose/streptozotocin induced type 2 diabetes in rats. Exploration of bioactive compounds using UHPLC-ESI-QTOF-MS. *Arch Physiol Biochem*. 2021. <https://doi.org/10.1080/13813455.2021.1921811>.
29. Yang J, Li H, Wang X, Zhang C, Feng G, Peng X. Inhibition mechanism of α -amylase/ α -glucosidase by silibinin, its synergism with acarbose, and the effect of milk proteins. *J Agric Food Chem*. 2021;69:10515–26.
30. Nanok K, Sansenya S. α -Glucosidase, α -amylase, and tyrosinase inhibitory potential of capsaicin and dihydrocapsaicin. *J Food Biochem*. 2020;44:e13099.
31. Quan NV, Xuan TD, Tran HD, Thuy NTD, Trang LT, Huong CT, Andriana Y, Tuyen PT. Antioxidant, α -amylase and α -glucosidase inhibitory activities and potential constituents of *Canarium tramdenum* bark. *Molecules*. 2019;24:605.
32. Abed SN, Bibi S, Jan M, Talha M, Islam NU, Zahoor M, Al-Joufi FA. Phytochemical composition, antibacterial, antioxidant and antidiabetic potentials of *Cydonia oblonga* bark. *Molecules*. 2022;27:6360.
33. Tungmunthum D, Thongboonyou A, Pholboon A, Yangsabai A. Flavonoids and other phenolic compounds from medicinal plants for pharmaceutical and medical aspects: an overview. *Medicines (Basel)*. 2018;5:93.
34. Jose M, Cyriac MB, Pai V, Varghese I, Shantaram M. Antimicrobial properties of *Cocos nucifera* (coconut) husk: an extrapolation to oral health. *J Nat Sci Biol Med*. 2014;5:359–64.
35. Abdollahzadeh E, Rezaei M, Hosseini H. Antibacterial activity of plant essential oils and extracts: the role of thyme essential oil, nisin, and their combination to control *Listeria monocytogenes* inoculated in minced fish meat. *Food Control*. 2014;35:177–83.
36. Zeghib W, Boudjouan F, Vasconcelos V, Lopes G. Phenolic compounds' occurrence in *Opuntia* species and their role in the inflammatory process: a review. *Molecules*. 2022;27:4763.
37. Chulrik W, Jansakun C, Chaichompo W, Aman T, Pathumwadee Y, Apsorn S, Wilanee C, Apichart S, Chunglok W. Oxocresbanine from *Stephania pierrei* exerts macrophage anti-inflammatory effects by downregulating the NF- κ B, MAPK, and PI3K/Akt signalling pathways. *Inflammopharmacol*. 2022;30:1369–82.
38. Toma L, Sanda GM, Niculescu LS, Deleanu M, Sima AV, Stancu CS. Phenolic compounds exerting lipid-regulatory, anti-inflammatory and epigenetic effects as complementary treatments in cardiovascular diseases. *Biomolecules*. 2020;10:641.
39. El-Halawany AM, Abdallah HM, Hamed AR, Khalil HE, Almohammadi AM. Phenolics from *Barleria cristata* var. Alba as carcinogenesis blockers against menadione cytotoxicity through induction and protection of quinone reductase. *BMC Complement Altern Med*. 2018;18:1–7.
40. Promraksa B, Phetcharaburanin J, Namwat N, Techasen A, Boonsiri P, Loilome W. Evaluation of anticancer potential of Thai medicinal herb extracts against cholangiocarcinoma cell lines. *PLoS ONE*. 2019;14:e0216721.
41. Manglani N, Vaishnava S, Dhamodaran P, Sawarkar H. In vitro and in vivo anticancer activity of leaf extract of *Barleria grandiflora*. *Int J Pharm Pharm Res*. 2014;6:70–2.
42. Atale N, Gupta S, Yadav UC, Rani V. Cell-death assessment by fluorescent and nonfluorescent cytosolic and nuclear staining techniques. *J Microsc*. 2014;255:7–19.
43. Baig MH, Ahmad K, Rabbani G, Danishuddin M, Choi I. Computer aided drug design and its application to the development of potential drugs for neurodegenerative disorders. *Curr Neuropharmacol*. 2018;16:740–8.
44. Wu X, Ding H, Hu X, Pan J, Liao Y, Gong D, Zhang G. Exploring inhibitory mechanism of gallic acid gallate on α -amylase and α -glucosidase relevant to postprandial hyperglycemia. *J Funct Foods*. 2018;48:200–9.
45. Alqahtani AS, Hidayathulla S, Rehman MT, ElGamal AA, Al-Massarani S, Razmovski-Naumovski V, Alqahtani MS, El Dib RA, AlAjmi MF. Alpha-amylase and alpha-glucosidase enzyme inhibition and antioxidant potential of 3-oxolupenol and katononic acid isolated from *Nuxia oppositifolia*. *Biomolecules*. 2019;10:61.
46. Dilshad R, Khan K-u-R, Saeed L, Sherif AE, Ahmad S, Ovatlarnporn C, Nasim J, Hussain M, Ghalloo BA, Basit A. Chemical composition and biological evaluation of *Typha domingensis* pers. to ameliorate health pathologies: In vitro and in silico approaches. *BioMed Res Int*. 2022;2022:8010395.
47. Al-Qahtani J, Abbasi A, Aati HY, Al-Taweel A, Al-Abdali A, Aati S, Yanbawi AN, Khan MA, Ghalloo BA, Anwar M. Phytochemical, antimicrobial, antidiabetic, thrombolytic, anticancer activities, and in silico studies of *Ficus palmata* forssk. *Arabian J Chem*. 2023;16:104455.
48. Türkan F, Taslimi P, Abdalrazaq SM, Aras A, Erden Y, Celebioglu HU, Tuzun B, Ağırtaş MS, Gülçin İ. Determination of anticancer properties and inhibitory effects of some metabolic enzymes including acetylcholinesterase, butyrylcholinesterase, alpha-glycosidase of some compounds with molecular docking study. *J Biomol Struct Dyn*. 2021;39:3693–702.
49. Daina A, Michielin O, Zoete V. iLOGP: a simple, robust, and efficient description of n-octanol/water partition coefficient for drug design using the GB/SA approach. *J Chem Inf Model*. 2014;54:3284–301.
50. Duffy FJ, Devocelle M, Shields DC. Computational approaches to developing short cyclic peptide modulators of protein–protein interactions, computational peptidology. New York: Springer; 2015. p. 241–71.
51. Lipinski CA. Lead-and drug-like compounds: the rule-of-five revolution. *Drug Discov Today Technol*. 2004;1:337–41.
52. Banerjee P, Eckert AO, Schrey AK, Preissner R. ProTox-II: a web-server for the prediction of toxicity of chemicals. *Nucleic Acids Res*. 2018;46(W1):W257–63.

Publisher's Note

Springer Nature remains neutral with regard to jurisdictional claims in published maps and institutional affiliations.